JGR Planets

RESEARCH ARTICLE
10.1029/2025JE008931

Geological History of the Dichotomy in the Southern Utopia Planitia of Mars

Tengfei Zhang[1], Jun Huang[1], Le Wang[1], Lukas Wueller[2], Wajiha Iqbal[2], Xiaozhong Ding[3], Long Xiao[1], and Harald Hiesinger[2]

[1]State Key Laboratory of Geological Processes and Mineral Resources, Hubei Key Laboratory of Planetary Geology and Deep Space Exploration, School of Earth Sciences, China University of Geosciences, Wuhan, China, [2]Institut für Planetologie, Universität Münster, Münster, Germany, [3]National Geological Mapping Research Center of China Geological Survey, Beijing, China

Key Points:

- We conducted high-resolution geological mapping in the dichotomy of southern Utopia Planitia on Mars (5°–30°N, 105°–115°E)
- Crater size-frequency distribution and cross-cutting relationships reveal the region's five-stage evolution, reflecting its complex geologic and resurfacing history
- $AHul_2$ meets Tianwen-3 constraints and preserves Hesperian water features, making it ideal for studying Mars' climate and hydrologic history

Correspondence to:
J. Huang,
junhuang@cug.edu.cn

Citation:
Zhang, T., Huang, J., Wang, L., Wueller, L., Iqbal, W., Ding, X., et al. (2025). Geological history of the dichotomy in the southern Utopia Planitia of Mars. *Journal of Geophysical Research: Planets*, *130*, e2025JE008931. https://doi.org/10.1029/2025JE008931

Received 5 JAN 2025
Accepted 30 JUN 2025

Abstract The Martian crustal dichotomy represents a fundamental geological boundary, separating the ancient Noachian highlands in the south from the relatively younger lowlands to the north, which may host sediments derived from a putative northern ocean. To investigate the tectonic and hydrologic evolution of this transition, we produced a high-resolution geologic map of the southern Utopia Planitia region (5°–30°N, 105°–115°E), identifying 20 stratigraphic units grouped into highland, transitional, lowland, Amenthes region, and impact-related categories. Chronostratigraphic constraints based on crater size-frequency distributions and cross-cutting/super-positional relationships allow division of the regional geologic history into five stages, encompassing two major extrusive episodes, two regional volcanic pulses, and one intrusive event. Wrinkle ridges concentrated in the central and southern mapping areas reflect compressional stresses likely associated with these volcanic events (e.g., Watters, 1988, https://doi.org/10.1029/jb093ib09p10236; Yin et al., 2023, https://doi.org/10.26464/epp2023031), suggesting that magmatic activity was a dominant driver of Noachian–Hesperian tectonic evolution. In contrast, Hesperian and Amazonian units in the northern region are interpreted as water-related deposits, consistent with emplacement in a volatile-rich environment. Among these, the $AHul_2$ unit satisfies both engineering and scientific criteria for landing, highlighting it as a favorable site for China's Tianwen-3 sample return mission. This study refines our understanding of the geological evolution across the dichotomy boundary and informs future exploration strategies.

Plain Language Summary Mars displays a prominent dichotomy, with ancient, elevated highlands in the south and younger, lower-lying plains in the north—regions that may have once hosted an ocean. To better understand the geological evolution of this boundary, we produced a detailed geologic map of southern Utopia Planitia (5°–30°N, 105°–115°E). We identified 20 surface units and grouped them into five categories: highland, transitional, lowland, Amenthes region, and impact crater units. Through crater size–frequency analysis and cross-cutting relationships, we reconstructed the geological history in five stages, revealing that both extrusive and intrusive activity played key roles. The $AHul_2$ unit, located in the northern lowlands, was mapped as part of the Vastitas Borealis Formation and is identified as a candidate landing site for the Tianwen-3 sample return mission. This study enhances our understanding of the regional geologic evolution near the Martian dichotomy and provides a framework for future exploration of Utopia Planitia.

1. Introduction

The topography of Mars is markedly dichotomous, divided into the southern highland and the northern lowland (e.g., Carr, 2007). Previous studies suggest that the northern lowlands were once covered by a standing body of water (Carr & Head, 2003; Clifford & Parker, 2001; Craddock & Howard, 2002; Dickeson & Davis, 2020; Parker et al., 1989, 1993). Parker et al. (1989, 1993) identified two sets of potential ancient shorelines using the Viking Orbiter images: the Arabia shoreline, which aligns with the dichotomy boundary, and the Deuteronilus shoreline, which corresponds to the edge of the northern lowland (Clifford & Parker, 2001). Head et al. (1999) analyzed two ancient shorelines on Mars using the Mars Orbiter Laser Altimeter (MOLA) data and found that the Deuteronilus shoreline is primarily located at the same equipotential surface. Ivanov et al. (2017) updated the global map of the Deuteronilus shoreline using daytime mosaicked infrared (IR) images from the Thermal Emission Imaging System (THEMIS). Sholes et al. (2021) focused primarily on the Deuteronilus Mensae region and used high-resolution CTX images to re-map the Arabian shoreline.

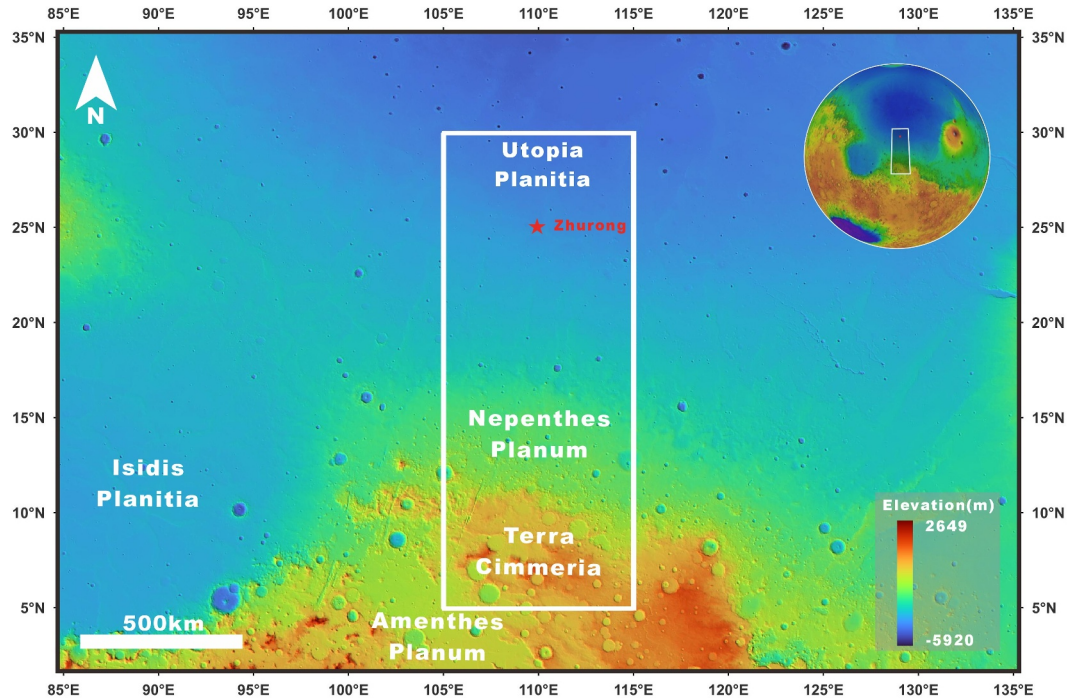

Figure 1. Regional topography of the study area. The red star is the Zhurong landing site. The base map is Mars Orbiter Laser Altimeter (MOLA; Smith et al., 2001) shaded relief map overlain with colour-coded MOLA elevation map.

These are crucial pieces of evidence for the hypothesis of an ancient northern ocean on Mars (Carr & Head, 2003; Clifford & Parker, 2001; Craddock & Howard, 2002; Dickeson & Davis, 2020; Palumbo & Head, 2019) that is further supported by the discovery of bidirectional cross-bedding (Xiao et al., 2023) and subsurface sedimentary layers by China's Zhurong rover (C. Li et al., 2022). The cross-bedding is indicative of a shallow marine depositional environment in the northern lowland (Xiao et al., 2023), while the subsurface sedimentary layers are potentially related to flood activities (C. Li et al., 2022).

Studying the geological conditions near the dichotomy boundary in the Utopia Planitia is critical for understanding the geological evolution history of the region, and the evolution of ancient oceans. This research can also provide valuable insights for future Mars exploration and sample return missions.

Therefore, we selected the area covering the Zhurong rover landing site (109.9°E, 25.1°N) to enhance our understanding of the geological history and ancient ocean evolution of the northern plains. The topography from north to south (Figure 1) includes: the northern Utopia Planitia, a flat and smooth northern plain with various structural features such as etched flows and polygons; Nepenthes Planum, located in the transition zone between the southern highlands and the northern lowlands, with some rough surface features and a general southward slope; Terra Cimmeria, an ancient southern highland with a rough and rugged surface; and Amenthes Planum, located in the southwestern region of the mapping area, a flat extrusive plain (Tanaka, Skinner, et al., 2014). In the geological map, we focused on distinguishing the geological boundaries and geomorphological features between different geological units, providing detailed identification and division of various geological regions to achieve a comprehensive understanding of the area's formation history.

We have finally produced a large-scale geological map (mapping scale 1:1,000,000), identifying various landforms formed during different stages of Mars' history.

2. Regional Setting

The study area (105°–115°E and from 5° to 30°N) is located near the dichotomy boundary in the southern region of Utopia Planitia and is tilted toward the north by approximately 0.16°. Utopia Planitia is in the northern part of the mapping area, Nepenthes Planum is in the central part, Terra Cimmeria is in the southern part, and Amenthes

Planum occupies a small southwestern portion of the mapping area (Figure 1). The chronostratigraphy shows an overall trend from older units in the south to younger units in the north of our mapping area, spanning large parts of martian history.

Northern Utopia Planitia formed during the Early Noachian period (Frey et al., 2002; Frey & Schultz, 1988; McGill, 1989; Solomon et al., 2005; Wilhelms, 1973). It is considered a large impact basin (McGill, 1989) and may have been a depositional center of fluvial, aeolian, and extrusive processes in the Late Noachian (Tanaka et al., 2005; Tanaka, Carr, et al., 2003; Tanaka, Skinner, et al., 2003; Tanaka, Skinner, et al., 2014; Carr, 1996; Greeley & Guest, 1987; Head, 2002; Kargel et al., 1995; Scott & Tanaka, 1986). During the Early Hesperian, Utopia Planitia was covered by lava, forming a wrinkle ridge plain (Head, 2002; Kreslavsky & Head, 2000). Subsequently, with the development of outflow channels, it was covered by the Vastitas Borealis Formation (VBF) (Tanaka et al., 2005). Studies by Ivanov et al. (2014) on Utopia Planitia explored the formation of etched flows and polygons, indicating the presence of significant water bodies in the past.

Nepenthes Planum is the transitional zone between the southern highlands and the northern lowlands, containing Noachian impact breccias, extrusive rocks, and Hesperian aprons formed by mass-wasted deposits (Tanaka, Skinner, et al., 2014). During its evolution, it was affected by mass wasting and "basal sapping of volatiles" (Tanaka et al., 2005). The subsurface of this area is believed to contain faults related to the formation of Utopia Planitia (Frey & Schultz, 1990; McGill, 1989; Nimmo & Tanaka, 2005; Tanaka, Skinner, et al., 2003). These faults may have controlled the regional accumulation of rocks and sediments, as well as the long-term capture and transport of groundwater and/or ice reservoirs (Skinner & Tanaka, 2007; Tanaka, Skinner, et al., 2003).

Southern Terra Cimmeria represents the southern highlands in the mapping area, having formed its current topography through a long process of erosion and modification. In their global geological map of Mars, Scott and Carr (1976) classified the rugged, crater-dense plains of Terra Cimmeria into the Noachian system. Tanaka, Robbins, et al. (2014) divided this unit into the Middle Noachian highland unit, characterized by moderately to highly degraded terrain formed from undifferentiated impact, extrusive, fluvial, and basin materials. The presence of numerous lobate scarps and wrinkle ridges indicates that this area has undergone tectonic contraction (Watters & Robinson, 1999).

The southwestern Amenthes Planum is a long, narrow, lava-filled flat area in the southern highlands, formed between ~3.5 Ga and ~3.2 Ga (Erkeling et al., 2011). The NNE-trending Amenthes Fossae is one of the pieces of evidence for extensional tectonic activity (Maxwell & McGill, 1988; Wichman & Schultz, 1989).

3. Data Sets and Mapping Technique

We used QGIS 3.28 for digital mapping at a scale of 1:1,000,000, on the basis of five individual data sets: (a) the Global Context Camera (CTX) Mosaic with a pixel scale of ~5 m/pix obtained from The Bruce Murray Laboratory for Planetary Visualization (Dickson et al., 2018; http://murray-lab.caltech.edu/CTX/); (b) THEMIS IR daytime and (c) THEMIS IR nighttime data with a pixel scale of ~100 m/pix (Christensen et al., 2004); (d) the High Resolution Stereo Camera (HRSC)-MOLA Blended Digital Elevation Model (DEM) with a pixel scale of ~200 m/pix (Fergason et al., 2018); (e) High Resolution Imaging Science Experiment (HiRISE) with a pixel scale of 0.25–1 m/pix (McEwen et al., 2007); and (f) Tianwen-1 Moderate Resolution Imaging Camera (MoRIC) Digital Orthophoto Map (DOM) data with a pixel scale of 76 m/pix (Liu et al., 2024).

Our map covers an area of approximately 820,000 square kilometers and spans 25° of latitude (lat 5 to 30°N) and 10° of longitude (long 105 to 115°E). The Global Context Camera (CTX) Mosaic provided images of the entire study area, which we used as a basis for identifying landforms and delineating geological units. THEMIS IR daytime and nighttime data were primarily used to analyze differences in the thermophysical properties of surface materials to distinguish units that have similar morphological features in CTX images. The HRSC-MOLA Blended DEM provided topographic references, allowing us to distinguish geological units based on changes in landform slopes. HiRISE offered limited high-resolution imagery, helping us identify micro-scale differences and characteristics of various geological units. The MoRIC DOM is used to observe landforms and produce geological maps (Figure A1).

To better determine the relationships between different geological units, we conducted crater size-frequency distribution (CSFD) measurements for several units (Figure A2). We used CTX images as the base map, selecting flat areas within each unit as dating regions. We excluded secondary crater clusters and chains as much as

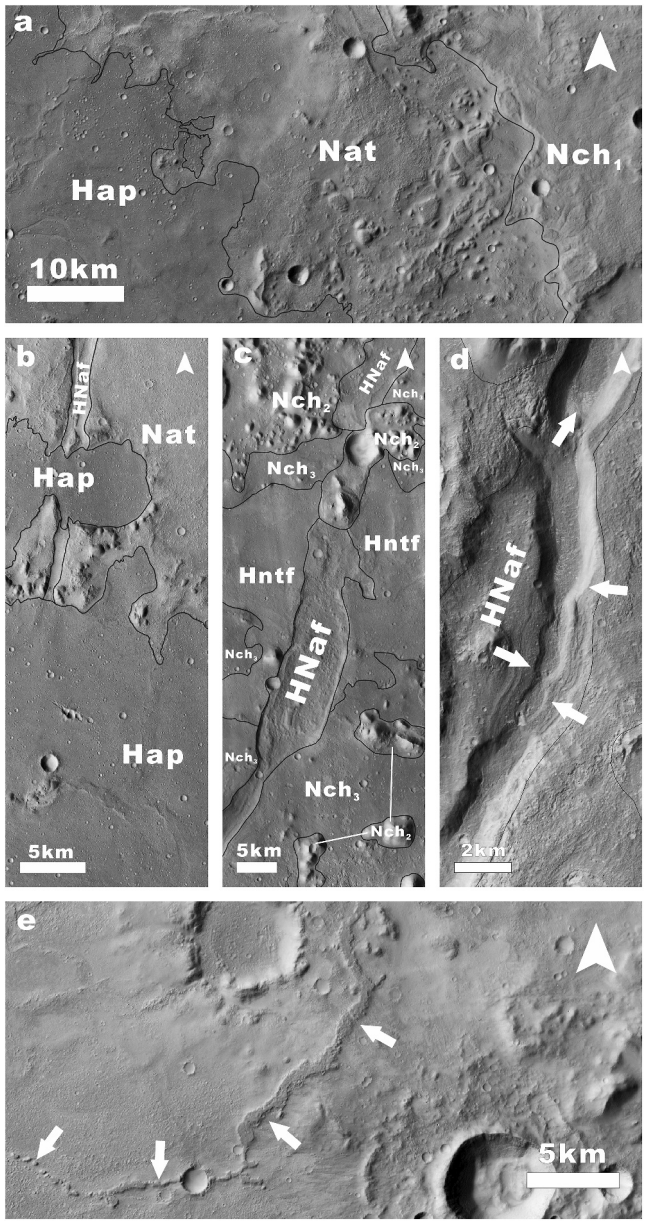

Figure 2. (a) The boundary among Hap, Nat, and Nch_1 with the central coordinates at 5.58°N, 106.04°E. (b) The overlapping relationships of Hap, Nat, and HNaf, centered at coordinates 6.24°N, 105.21°E. (c) The boundary of HNaf with Hntf, Nch_3, and Nch_2 with the central coordinates at 12.19°N, 107.75°E. (d) The secondary terraces in the HNaf grabens with the central coordinates at 11.52°N, 107.08°E. (e) Inverted channels within the Nat unit of the Amenthes region with the central coordinates at 6.77°N, 105.74°E. The base map is the global mosaic of CTX.

possible, identifying all craters within the dating regions with diameters no less than 100 m. CSFD measurements were used to estimate the absolute model ages of geological units based on the spatial density of impact craters (e.g., Hartmann, 1973; Hartmann & Neukum, 2001; Ivanov, 2001). Selected count areas were confined to individual geological units and were sufficiently large to ensure statistical reliability. Crater diameters were measured in QGIS using the OpenCraterTool plugin (Heyer et al., 2023), with efforts made to exclude secondary crater chains and clusters. CraterStats (https://github.com/ggmichael/craterstats) (Michael, 2013; Michael et al., 2012, 2016; Michael & Neukum, 2010) was employed to generate CSFD plots and to fit the Ivanov (2001) production function and the Hartmann and Neukum (2001) chronology function.

To enhance the comparability of this map with previous maps, we referred to the symbol standards of the Federal Geographic Data Committee (FGDC, 2006) and the terminology of the International Astronomical Union (IAU) (https://planetarynames.wr.usgs.gov/DescriptorTerms). The colors and naming conventions used in the geological map were modified following the schemes established in previous maps (Ivanov et al., 2014; Skinner & Tanaka, 2018). The naming convention for geological map units is as follows: epoch (Noachian, Hesperian, Amazonian); region; type; subdivision number. For example, "$AHul_3$" where "AH" represents the Hesperian to Amazonian, "u" stands for Utopia, "l" indicates the lowland unit, and "3" is the geomorphological classification number.

4. Results

We produced a comprehensive geological map of the region at a mapping scale of 1: 1,000,000 (Figure A1) using various data sets described above, in order to identify and characterize the geologic units and the geomorphic features. In our map, we have recognized 20 units, which have been grouped according to their geographic distribution as follows: three units in the Utopia region of the lowland area, two units in the Nepenthes Planum of the transitional area, four units in the Terra Cimmeria of the highland area, three units in the Amenthes region, and eight impact crater units.

4.1. Amenthes Region Units

Nat—Transitional unit—Forming the transition zone between Amenthes Planum and Terra Cimmeria (Figure 2a), this region contains several curved ridges (Figure 2e). The surface is rough with well-developed gullies. THEMIS data show overall high thermal inertia that is locally heterogeneous. The area is heavily degraded. There is a distinct escarpment with a vertical displacement of ~210 m, marking the boundary with the Amenthes Fossae unit (HNaf).

Interpretation: The inverted channels may have formed from active fluvial processes during the Noachian period, indicating liquid surface water in the past. This unit lies between the highlands and the extrusive plains, serving as a transitional zone between the two. Because this unit is cut by the Amenthes Fossae unit (HNaf), it predates the formation of the Amenthes Fossae unit (HNaf).

We suggest that during the Late Noachian, the southern glaciated highlands were modified by extrusive activity that formed the Nat unit near the Amenthes Planum. The surface still preserves chaotic terrain (Figure 2a). According to the research by Meresse et al. (2008), subsurface intrusive activity ultimately leading to the loss of groundwater is the primary cause of the formation of chaotic terrain. Additionally, extrusive activity potentially

liberated meltwater that formed the channels in unit Nat. Subsequently, the erosion removed the materials surrounding the channels and because deposits within the channels are more resistant, they appear as inverted channels (Figure 2e), and the fine-grained material produced by erosion was preserved in the low-lying areas of the unit.

Hap—Plains unit—The flat and smooth plains are part of the Amenthes Planum (Figure 2a). Numerous wrinkle ridges can be observed. In the mapping area, these wrinkle ridges can be up to about 26 km long and have two main orientations, NE-SW and NW-SE. This unit fills and cuts through the Amenthes Fossae unit (HNaf) (Figure 2b). Stream-islands and channels are visible and show lower temperatures than surround terrains in THEMIS IR nighttime images.

Interpretation: The Amenthes plains unit (Hap) is approximately 3.5 to 3.2 Ga old (Erkeling et al., 2011). During the Late Noachian, extensive interactions between lava and ice caused significant modification (e.g., Meresse et al., 2008) of the Nat unit, with the eroded sediments being deposited into the Amenthes Planum. In the Hesperian period, due to active extrusive activity, this area was filled with lava (Erkeling et al., 2011), covering parts of Nat and Noachian sediments and cutting through HNaf (Figure 2b). Upon the tectonic compression by the cooling of lava, the extrusive plains formed wrinkle ridges (Watters, 1988). The presence of sinuous channels distributed across the surface is indicative of past fluvial activity. Later, the surface was potentially covered by dust as indicated by the lower temperature than surrounding terrains in the THEMIS IR nighttime data.

HNaf—Fossae unit—Amenthes Fossae, intersecting multiple geological units (Figures 2b and 2c), this feature consists of a series of graben trending northeast-southwest. These grabens can be up to about 264 km long, 9 km wide, and 1 km deep in the mapping area. In the northern part, some terraces within the graben can be observed. The interiors of the grabens are smooth and contain secondary terraces (Figure 2d). In THEMIS IR nighttime data, the unit exhibits relatively lower temperatures compared to the surrounding terrains.

Interpretation: Maxwell and McGill (1988) suggest that the Amenthes Fossae unit (HNaf) itself is a potential source of igneous rock. According to Erkeling et al. (2011), Amenthes Fossae cuts through materials with model ages of ≥3.7 Ga from the Noachian and Hesperian periods but it does not cut through ∼3.6 Ga Hesperian impact craters and extrusive plains. In our study area, Amenthes Fossae cuts through Nch_2, Nch_3, and Nat (Figures 2b and 2c), all of which formed in the Late Noachian, with Nch_3 having a model age of 3.89 Ga. At the southern edge of the Amenthes Fossae unit (HNaf), channels are truncated and filled by the Amenthes plains unit (Hap), indicating that the formation of the Amenthes plains unit (Hap) postdates HNaf, with the filling of Amenthes Planum occurring between ∼3.5 and ∼3.2 Ga ago (Erkeling et al., 2011). Based on cross-cutting relationships of HNaf dissecting the Hesperian Nepenthes transitional flow unit (Hntf) with a model age of 3.71 Ga (Figure 2c), we infer that the graben was formed ∼3.71 Ga ago.

Amenthes Fossae are not confined to the mapped area of this study but are also distributed more broadly across the Circum-Isidis region. These grabens, formed under extensional tectonic regimes, may be linked to gravity anomalies associated with the interior structure of Isidis Planitia (Ritzer & Hauck, 2009).

In summary, the grabens of unit HNaf formed during the Late Noachian, around ∼3.71 Ga, and may be associated with gravity anomalies within the interior structure of Isidis Planitia (Ritzer & Hauck, 2009).

4.2. Highland Region Units

The geological units in the southern Terra Cimmeria region mainly formed during the Noachian epoch, preserving inverted channels and small-scale reticulate ridges.

Nch_1—Noachian Cimmeria Highland unit 1—Located in the southern part of the mapped area (Figure 3), this unit is a significant component of the ancient Terra Cimmeria and is the oldest unit in the entire mapping area. It features very high relief outcrops (Figure 4a) that can extend hundreds of kilometers, with strata thickness potentially reaching several hundred meters (Tanaka, Skinner, et al., 2014). It contains numerous ancient impact craters up to about 72 km in diameter. Compared to Cimmeria highland unit 2 (Nch_2), Cimmeria highland unit 1 (Nch_1) has been less modified and is therefore more pristine. It has less gullies and depressions, and is not cut or divided by them. In THEMIS images, the thermal inertia distribution is relatively uniform and generally low. There are scarps at the boundaries with other units.

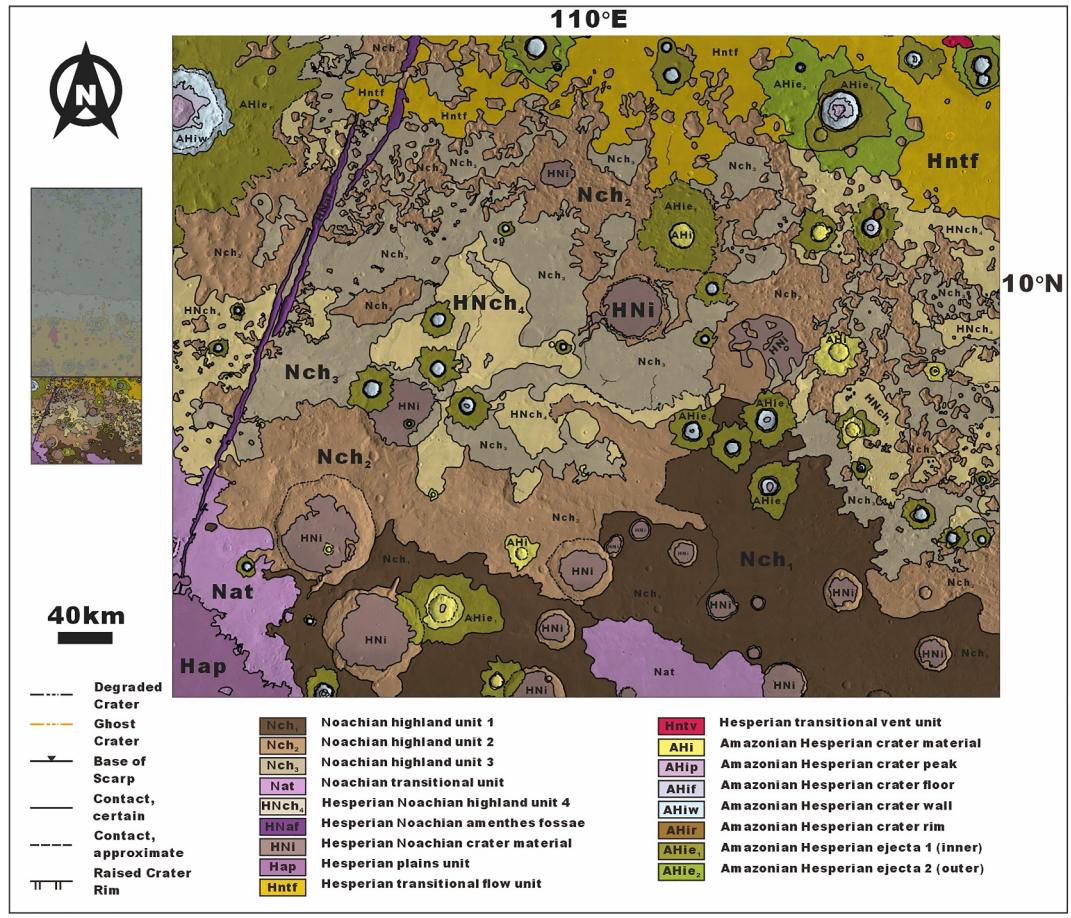

Figure 3. Geologic map of the Cimmeria highland region and the Amenthes region. The geological units in this area are complexly distributed, and the terrain is rugged. Amenthes Fossae cuts through multiple geological units from the Noachian to the Hesperian epochs. Most of the severely degraded impact craters in the fill region are located within this area. The basemap is the Moderate Resolution Imaging Camera.

Interpretation: We interpret this as Early Noachian material, consisting of ancient impact breccias formed after the formation of Utopia Planitia (Skinner & Tanaka, 2018). In the global geologic map (Tanaka, Skinner, et al., 2014), this area corresponds to the Early Noachian highland unit. The material is composed of undifferentiated impact, extrusive, aeolian, fluvial, or lacustrine deposits with localized degradation or deformation (Tanaka, Skinner, et al., 2014). In our mapping area, we observe that this ancient geological unit has been modified by impacts and water activity, with impact craters that lack central peaks and ejecta, as well as (inverted) meltwater channels.

Although Nch_1 is the oldest unit in the mapping area, it is paradoxically less dissected than the adjacent Late Noachian units (Nch_2, Nch_3, Nat). This can be attributed, in part, to its composition: Nch_1 consists of Early Noachian impact megabreccia (Skinner & Tanaka, 2018), which imparts high mechanical competence and resistance to erosion. Furthermore, no chaotic terrain—typically associated with subsurface volatile loss (Chuang, 2015; Meresse et al., 2008; Sharp, 1973)—has developed within Nch_1, suggesting that its structural integrity has remained largely intact over time. In contrast, units such as Nch_2 exhibit chaotic terrain, where fracturing due to volatile release weakens the substrate, reducing its resistance to erosion and enhancing subsequent degradation (Squyres, 1978).

This unit once contained significant amounts of ice, forming the southern glaciated highlands (Fastook & Head, 2015). During the Late Noachian, it was affected by large-scale extrusive and intrusive activity, leading to modification into Nch_2, Nch_3 and Nat units by the groundwater loss, with chaotic terrain visible in some areas

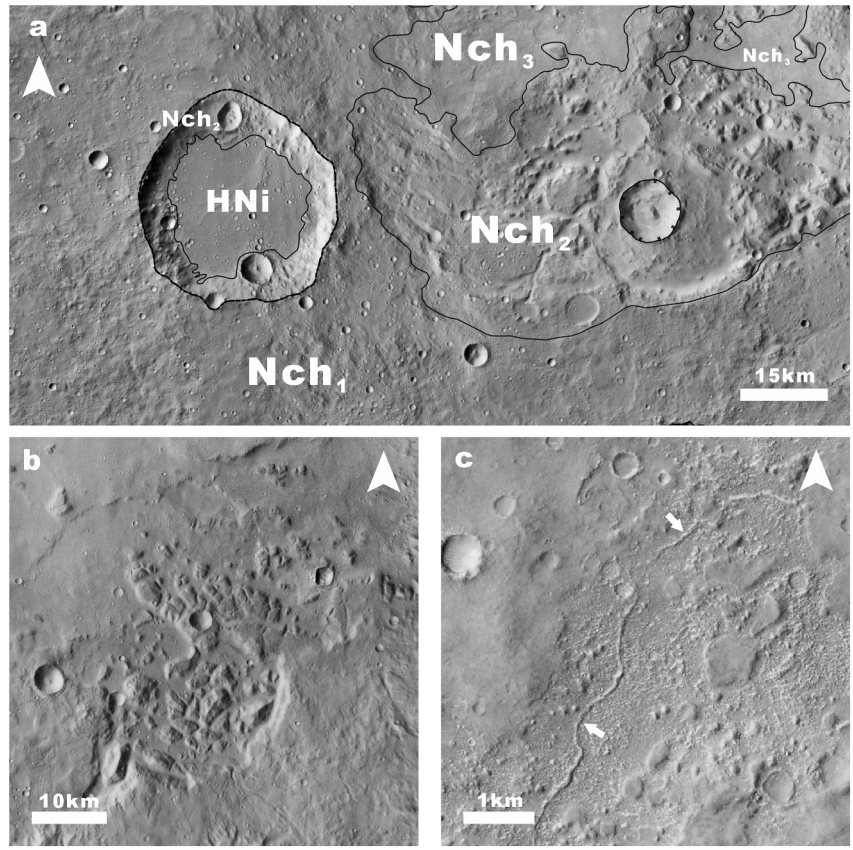

Figure 4. (a) The boundaries among Nch_1, Nch_2, and Nch_3 with the central coordinates at 6.41°N, 113.70°E. (b) The chaotic terrain within the Nch_2 unit, with the CTX mosaic as the base map (centered at 8.31°N, 106.68°E). (c) The (inverted) meltwater channels on the Nch_1 unit, with the CTX mosaic as the base map (centered at 5.93°N, 114.67°E).

(Figure 4b). Additionally, the increased local temperatures from extrusive activity likely caused the glaciers in the highlands to melt, forming (inverted) meltwater channels in some locations (Figure 4c). We believe that surface glaciers were present on a small scale, as the distribution of meltwater channels is not widespread.

Nch_2—Noachian Cimmeria Highland unit 2—The hummocky terrain on Terra Cimmeria was separated from the Cimmeria highland unit 1 (Nch_1) using erosional processes. It features clusters of small hills with varying shapes and significant dust accumulation between them, as observed in THEMIS data. Additionally, it is characterized by numerous intersecting gullies, dividing the surface into many fragmented plateaus and small hills (Figures 4a and 5a). THEMIS IR nighttime images show lower temperatures than surrounding terrains.

Interpretation: We interpret this unit as the erosional remnants of the Late Noachian glaciated highlands. This unit is geographically closely related to Nch_1 and Nch_3. The (inverted) meltwater channels found on the surface of Nch_1 (Figure 4c) indicate the presence of ancient glaciers, while the wrinkle ridges found on Nch_3 (Figure 5b) suggest extrusive activity in the area. The main landforms of Nch_2 are fragmented mesas and small hills, appearing in clusters or isolated, along with some rugged slopes.

Sharp (1973) identified the fretted terrain and chaotic terrain on Mars using images from Mariner 6 and Mariner 9, and found that they are primarily distributed in the equatorial and mid-latitude regions. Sharp (1973) proposed that fretted terrain originates from the progressive retreat of its own steep bounding cliffs—features that are integral to the unit itself—driven by processes such as sublimation of ground ice and/or groundwater-sapping erosion. Chaotic terrain, geographically associated with fretted terrain, is a rough terrain characterized by chaotic, irregularly arranged landforms of varying sizes, primarily caused by localized collapse due to the removal of subsurface materials (such as underground ice or magma) (Sharp, 1973). Squyres (1978) studied the

10.1029/2025JE008931

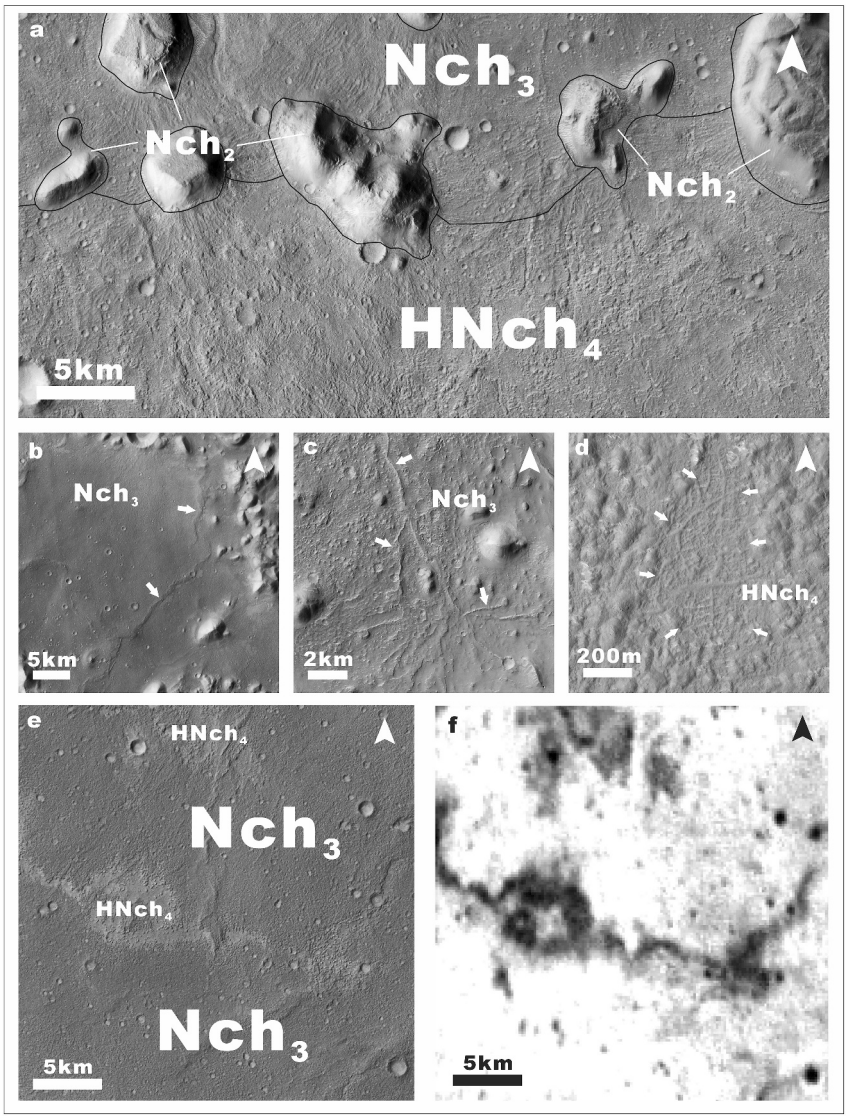

Figure 5. (a) The boundary between Nch_3 and $HNch_4$ with the central coordinates at 9.56°N, 114.64°E. (b) The wrinkle ridges on Nch_3, with the base map also being the CTX global mosaic, are centered at coordinates 11.45°N, 111.94°E. (c) The ridges on the southern highlands Nch_3, with the base map being the CTX global mosaic, are centered at coordinates 10.54°N, 110.37°E, adapted from Skinner and Tanaka (2018). (d) Reticulate ridges within the $HNch_4$ unit of the Terra Cimmeria Highlands (central coordinates 12.66°N, 106.94°E), with the base map from High Resolution Imaging Science Experiment (ESP_054656_1930). (e) Geomorphological variations between $HNch_4$ and Nch_3 units, with the basemap being CTX global mosaic, the central coordinate is 12.54°N, 106.99°E. (f) Night time temperature variations in $HNch_4$ and Nch_3 units, with the basemap being THEMIS IR nighttime global mosaic, the central coordinate is 12.54°N, 106.99°E.

linear features within fretted terrain and suggested that they resemble rock glaciers on Earth, possibly formed by the movement and deformation of ice and debris. Meresse et al. (2008) suggested that chaotic terrain might have resulted from localized collapse due to subsidence and extrusive activity. Chuang (2015) further noted that the deformation of fretted terrain could be linked to the sublimation of subsurface ice or the flow of ice-rich materials. Sharp (1973) also speculated that chaotic terrain could eventually evolve into fretted terrain as chaotic terrain is often geographically associated with fretted terrain, and in many places, chaotic terrain gradually transitions into fretted terrain.

Nch_2 is a hummocky geomorphological unit located in Terra Cimmeria, which we classify as fretted terrain. In some areas, chaotic terrain is observed to have been fragmented into mesas of varying sizes. In some regions,

magma erupted to the surface, the tectonic compression by the cooling of lava formed wrinkle ridges. This process caused surface collapse, leading to the formation of fractures and eventually chaotic terrain. As erosion progressed, it resulted in the development of fretted terrain, which is represented by the hummocky topography of Nch_2. Based on landforms associated with intrusive and extrusive activity, we propose that subsurface magmatism was a major geological process in Terra Cimmeria during the Noachian period, resulting in the loss of subsurface ice or water.

CSFD measurements of unit Nch_3 indicate that extrusive activity increased 3.89 Ga ago in the Late Noachian period. Lava eruptions, caused intense erosion of the surface, resulting in the chaotic terrain observed as fragmented mesas (Figure 4b). Subsequently, plateaus were eroded either forming small hills or becoming absent. According to Erkeling et al. (2011), Amenthes Fossae formed at approximately 3.7 Ga, whereas our CSFD results indicated that the Nch_2 unit formed around 3.89 Ga. This implies that, after an interval of ∼0.19 Ga, Amenthes Fossae developed as a graben system cutting through the Nch_2 unit.

Nch_3—Noachian Cimmeria Highland unit 3—The surface of this unit is characterized by a flat but rough texture (Figures 4a and 5a), and features wrinkle ridges and inverted channels (Figures 5b and 5c). THEMIS IR nighttime data shows higher temperature than $HNch_4$ unit. Located in the plains or depressions between the northern hills of Terra Cimmeria, it features smooth, low hills, narrow elongated gullies, and winding wrinkle ridges.

Interpretation: We suggest that this unit is an intermontane extrusive plain from the Late Noachian. Although Skinner and Tanaka (2018) suggest that it is a weathered layer of the highlands, composed of various undifferentiated impact units and degraded sedimentary plains formed by fluvial, colluvial, or lacustrine processes, we lean toward an extrusive origin. According to our CSFD measurements, this unit has a model age of approximately 3.89 Ga.

In the Late Noachian, extrusive activity or obliquity of Mars terminated the glaciation phase in the highlands (Montmessin, 2007), modifying the highlands in the south of our study region. The eroded material was mixed with lava and deposited in the flat plains and depressions between the hills of the southern highlands. Upon the tectonic compression by the cooling of lava, the lava contracted and formed wrinkle ridges (Figure 5b). The active extrusive processes melted the glaciers of the southern highlands, liberating large volumes of meltwater and eventually forming inverted channels (Figure 5c).

During the Hesperian, the formation of Hntf covered the potentially existing Nch_3 unit in the north, and the Nch_3 unit in the southern highlands was modified.

$HNch_4$—Hesperian and Noachian Cimmeria Highland unit 4—Located in the northern part of Terra Cimmeria, this unit is characterized by a hummocky surface (Figure 5a) and includes impact craters up to 6,000 m in diameter. THEMIS IR nighttime data show lower thermal inertia relative to surrounding terrains (Figure 5f). CTX imagery reveals densely distributed, small, smooth hills in certain areas (Figure 5e). The contact with Cimmeria Highland Unit 3 (Nch_3) varies spatially, transitioning from a well-defined (certain) boundary to an approximate one. HiRISE images show the presence of reticulate ridges (Figure 5d), some of which reach lengths of ∼900 m and widths of up to ∼30 m, with the broadest ridge systems extending as wide as ∼400 m.

Interpretation: This unit dates to the Late Noachian to Early Hesperian period. It exhibits a hummocky surface mantled by fine-grained materials, such as dust, and contains localized collapse or erosional features. In areas where the boundary is more distinct, small hills a few meters in height can be observed.

Skinner and Tanaka (2018) proposed that this area originated from fluvial or lacustrine deposition followed by degradation. Our CSFD measurements yielded an age of ∼3.66 Ga, placing the unit within the Hesperian. We interpret its formation as primarily the result of erosional processes driven by lava or water. Ye et al. (2019) suggested that high-salinity brines could lead to the development of reticulate ridges through evaporative processes. Accordingly, we interpret the ridges observed in this unit (Figure 5d) as features associated with past fluvial activity.

The $HNch_4$ unit is mantled by a substantial layer of dust, which contributes to its lower nighttime temperatures relative to surrounding terrains, as observed in THEMIS IR data (Figure 5f).

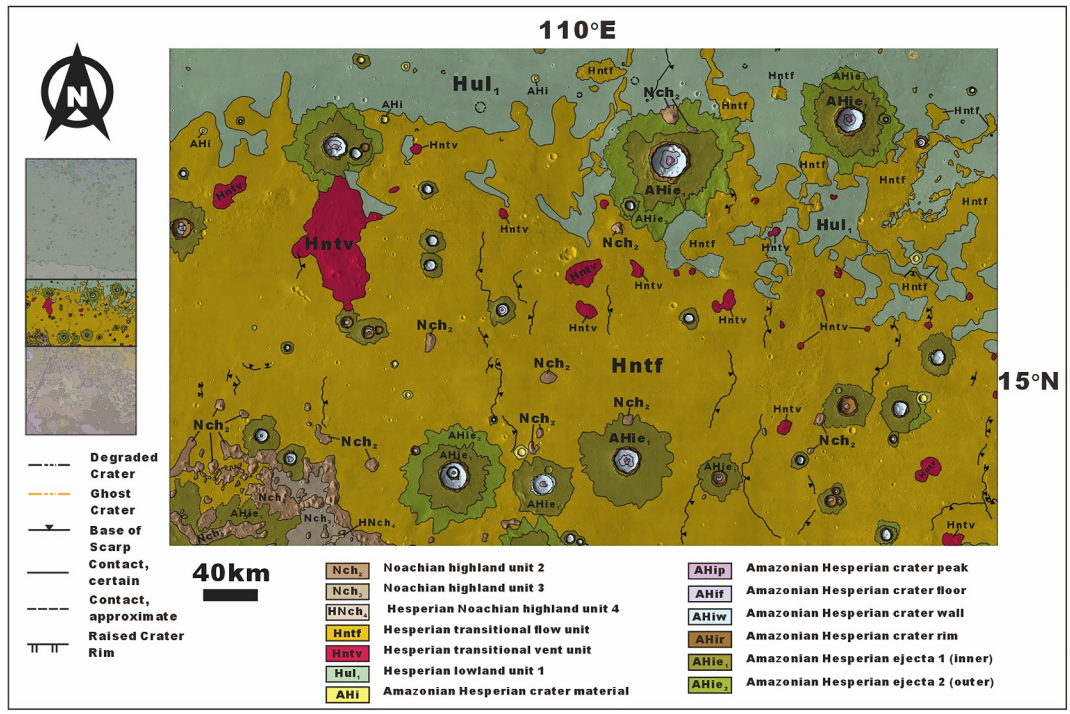

Figure 6. Geologic map of the Nepenthes transitional region with basemap is the Moderate Resolution Imaging Camera. The terrain is relatively flat, with some north–south trending wrinkle ridges visible in the region. Large impact craters exhibit well-preserved structures, and distinct double-layer ejecta can be observed.

4.3. Transitional Region Units

The geological units of Nepenthes Planum primarily formed during the Hesperian epoch, with its unique rough surface texture possibly indicating special mechanisms during its formation and evolution.

Hntf—Transitional flow unit—This unit is located in the transitional zone (Figure 6) between Utopia Planitia and Terra Cimmeria, specifically in the Nepenthes Planum region, with a latitude range approximately between 12°N and 18°N. Amenthes Cavi are located along the northern boundary of this unit (Brož & Hauber, 2013; Skinner & Tanaka, 2007). Rugged surface consists of rough terrain (Figure 7a) and north-south oriented wrinkle ridges (Figure 7c). The southern edge of the unit is more fragmented, interwoven with Cimmeria highland unit 4 ($HNch_4$), Cimmeria highland unit 3 (Nch_3), and Cimmeria highland unit 2 (Nch_2). In the center of the unit, there are some small hills and plateaus originating from Nch_2. Near the northern boundary of the Hntf unit, small cones with central pits are observed.

Interpretation: We interpret this unit as a mixture of lava flows and mudflows from the Early Hesperian epoch. Lava or sediment flows were ejected from large conical depressions in the Nepenthes transitional vent unit (Hntv). Various episodes of eruptions and erosions have created surface features varying from rugged to smooth surface textures. The transition with Hntv indicates a contemporaneous origin, with its formation period dating back to the Early Hesperian (Skinner & Tanaka, 2018), and our CSFD measurements (Figure A2) suggest an age of approximately 3.71 Ga. This unit is interpreted as being composed of erupted sheet lavas, mudflows, or a combination of both (Tanaka, Skinner, et al., 2003). The rough surface texture of the Nepenthes transitional flow unit (Hntf) may be due to differences in material sources and subsequent environmental variations (e.g., drying, contraction, or wind erosion; Skinner & Tanaka, 2018).

We propose that extrusive or intrusive activity played a significant role in the formation of this unit. On one hand, the widespread conical depressions within the unit may be extrusive craters, while the numerous north-south ridges are interpreted as wrinkle ridges, likely formed by the tectonic compression by the cooling of lava and contraction of an extrusive plain.

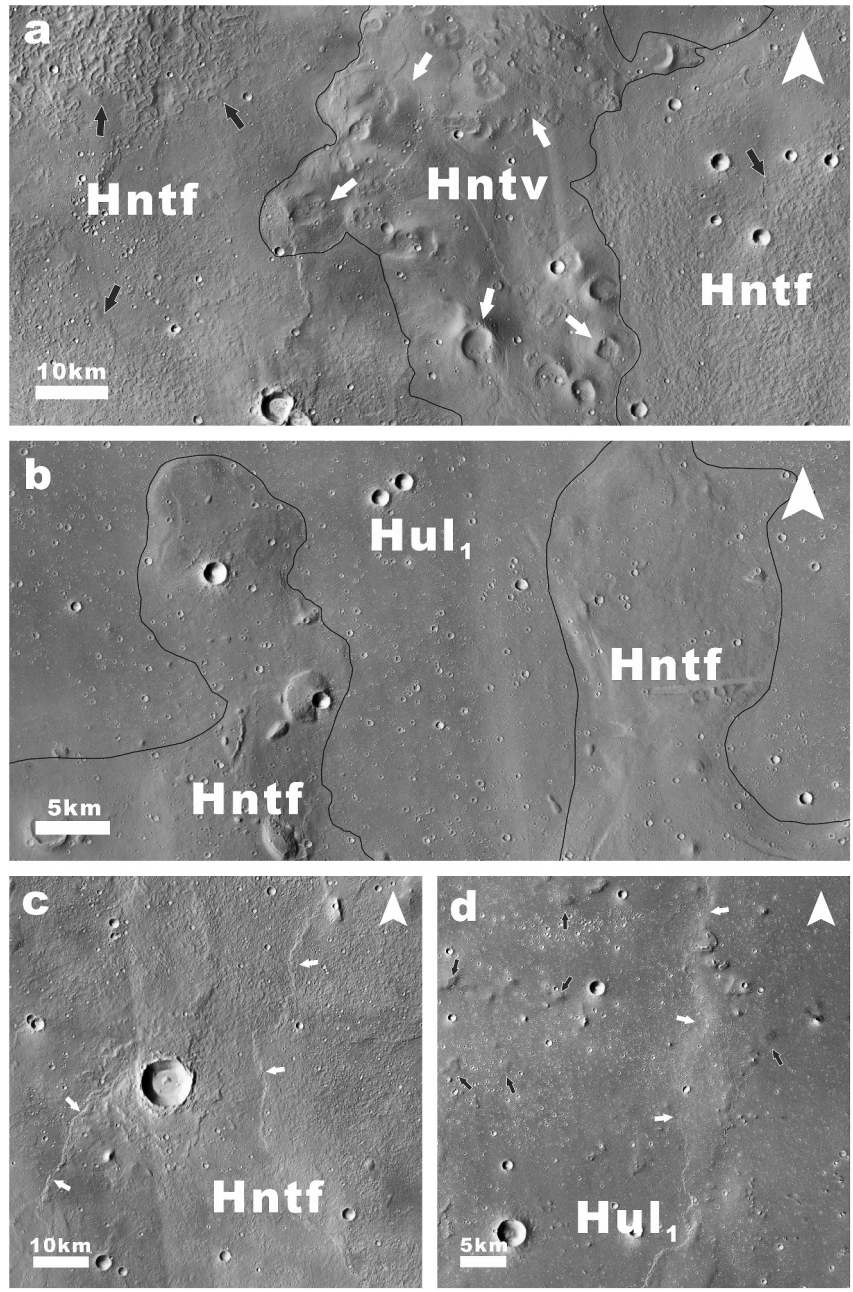

Figure 7. (a) The boundary between Hntv and Hntf, where the white arrows point to the extrusive vent of the Hntv unit, and the black arrows point to the rough textured structures on Hntf, with the central coordinates at 16.61°N, 106.99°E. (b) The boundary between Hul_1 and Hntf, with the central coordinates at 18.11°N, 109.49°E. (c) The ridges on Hntf that are not covered are indicated by the white arrows, with the central coordinates of 13.82°N, 111.82°E. (d) The Hul_1 unit covers other landforms; the white arrows indicate coverage over the lower ridges, while the black arrows indicate coverage over the plateau and small hills, with central coordinates of 19.42°N and 111.40°E. The base maps of (a)–(d) are the CTX global mosaic.

Additionally, the Nepenthes transitional vent unit (Hntv) suggests an eruption type (interaction of magma and surface or subsurface water), similar to tuff cones on Earth, indicating the presence of water or ice in the subsurface at the time of extrusive activity. The rough surface texture is attributed to the liberation of subsurface volatiles (Skinner & Tanaka, 2018). We suggest that groundwater migrating northward seeped to the surface and

modified it. The presence of large impact craters with lobate ejecta indicates that this area was once rich in water or ice (Weiss & Head, 2015).

There are irregular depressions in the northern part of Hntf, which we believe were caused by subsurface magma activity in the Hesperian period (Brož & Hauber, 2013; Tanaka, Carr, et al., 2003). This activity likely led to the melting of the permafrost layer, causing sediment migration northward and resulting in surface subsidence. The magma may have ascended through fractures formed during the creation of the Utopia Basin.

In summary, we propose that during the Early Hesperian period, a second large-scale intrusive event occurred in the mapped area. Extensive flows of lava covered water-bearing sediments in Nepenthes Planum, forming numerous north-south wrinkle ridges upon the tectonic compression by the cooling of lava. The interaction of lava with sediments led to eruptions resulting in rough surface texture (Skinner & Tanaka, 2018). After emplacement, the Hntf was cut by the second phase of tectonic activity that formed a long graben, referred to as Amenthes Fossae (HNaf).

Hntv—Transitional vent unit— Located on the Nepenthes Planum and primarily distributed within the Nepenthes transitional flow unit (Hntf), the surface of the transitional vent unit (Hntv) is smooth and features prominent small hills with central depressions or pits. The small hills can be up to about 300 m high and depressions up to about 200 m deep. Multiple small hills and depressions may be present within the same unit area (Figure 7a).

Interpretation: We interpret this as extrusive material formed during the same period as the Nepenthes transitional flow unit (Hntf). The small hills with depressions within the unit may be volcanoes, and the depressions could be former calderas. These hills vary in size.

Brož and Hauber (2013) measured the geometry of these cones in detail and suggested that the large conical depressions in Nepenthes Planum are of intrusive origin as their morphology resembles terrestrial tuff rings or tuff cones, formed by steam explosions resulting from interactions between lava or magma and surface or subsurface water. This interaction leads to explosive extrusive eruptions, ejecting large volumes of extrusive debris and creating wide extrusive craters. These tuff cones are mainly distributed in the northern part of Hntf, but there is no significant correlation between their size and location.

4.4. Lowland Region Units

The geological units in the northern region of the map mainly formed during the Hesperian and Amazonian epochs, featuring small-scale landforms such as mesas, pitted cones, and mud volcanoes, closely related to water and intrusive activities.

Hul_1—Lowland unit 1—This unit is located on the southern edge of Utopia Planitia, bordering Nepenthes Planum (Figure 8). The area is generally flat and smooth, with low hills and north-south trending scarps (Figure 7b), featuring an average slope of 0.423°, an elevation ranging from −4,022 m to −2,908 m, and an average elevation of −3,458 m. Several partially buried craters are present, characterized by exposed crater rims, while the remaining crater structures are covered and infilled by materials from Utopia Lowland Unit 1 (Hul_1). The southern part contacts the Nepenthes Transitional Flow Unit (Hntf), and it is significantly lower in elevation than Hntf, with noticeable slope and elevation changes at the boundary. This boundary, situated at an elevation of approximately −3,300 m, marks a distinct slope break separating the Hul_1 and Hntf units. It covers some mesas from Hntf, which may reach tens to hundreds of meters in height.

Interpretation: We suggest that this area is composed of mud debris flows, primarily formed during the Hesperian. In THEMIS IR nighttime images, this area is not significantly different from $AHul_2$ and may consist of sediments similar to the VBF. In the global geological map of Mars (Tanaka, Skinner, et al., 2014), it was identified as a Hesperian deposit consisting of rock collapses, fluvial/lacustrine sediments, and possibly other sediments and igneous rocks, with tectonic contraction in some places. The origin may be sedimentary or low-viscosity lava flows (Skinner & Tanaka, 2018).

Amenthes Cavi is located in the southern part of this unit and has a maximum depth of about 100 m. According to Skinner and Tanaka (2007), mud volcanism caused fine-grained materials from depth within the crust to move upward to the surface and then settle due to source depletion, forming Amenthes Cavi. In this region, we can observe some impact craters with well-preserved crater rims, indicating a low rate of erosion. Based on CSFD

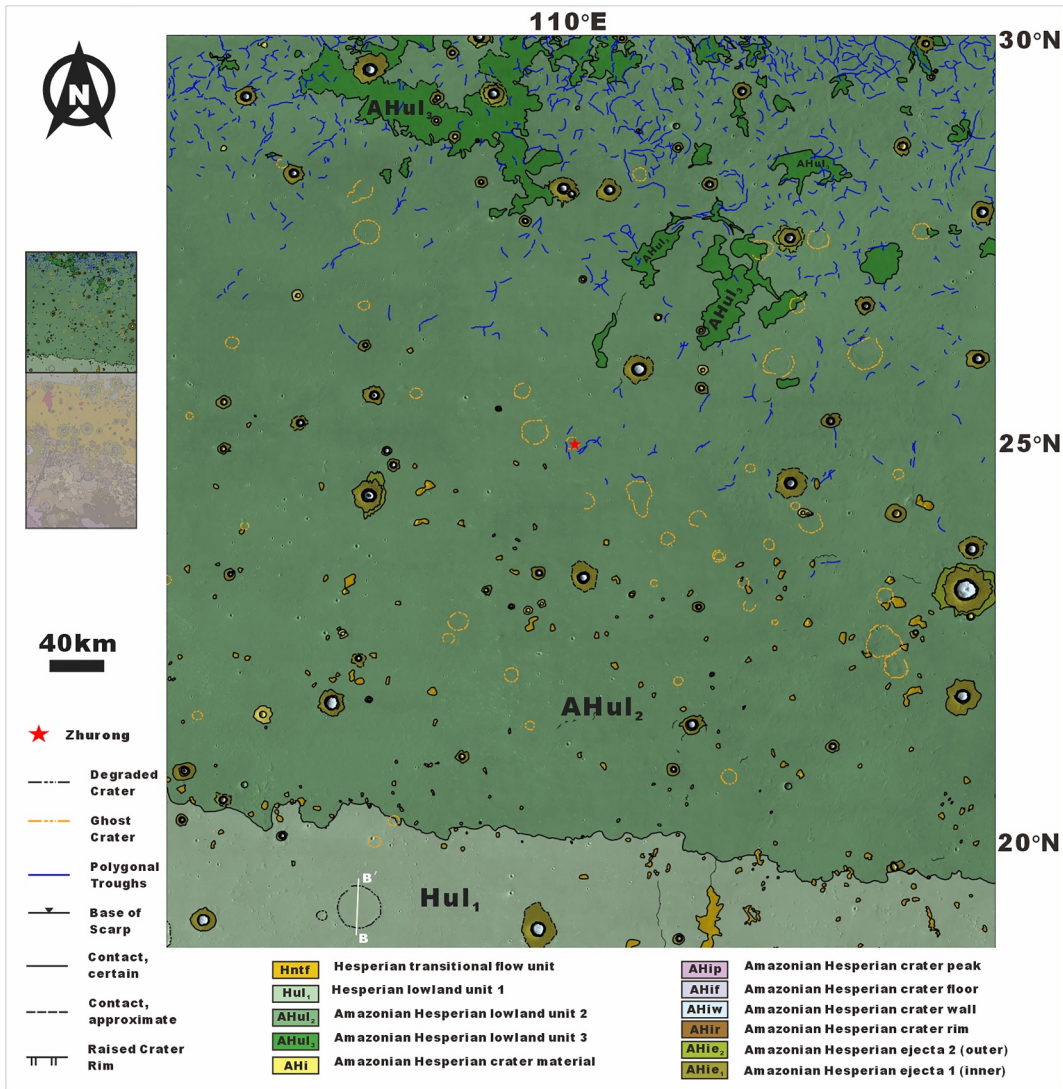

Figure 8. Geologic map of the Utopia Lowland Region units. The terrain is flat, primarily composed of geological units from the Hesperian to Amazonian epochs, and is characterized by a large number of ghost craters (Buczkowski & Cooke, 2004) and polygonal terrain. The base map is the Moderate Resolution Imaging Camera.

measurements, this unit has a model age of 3.63 Ga (Figure A2), placing it in the Hesperian. We propose that underground intrusive activity may have caused the permafrost layer to melt, forming debris flows that moved northward into Utopia Planitia, covering isolated mesas of Hntf and wrinkle ridges formed by the Hntf unit along the way (Figure 7d). The loss of material in the Amenthes Cavi area led to subsidence and the formation of depressions. This unit may extend beneath the Vastitas Borealis interior unit (Tanaka et al., 2005), but its exact termination point is unknown.

In this unit, there are several large partially filled impact craters with their rims exposed above the surface (Figure 9a). By comparing the calculated geometric parameters, such as crater depth, with actual measurements, we can estimate the thickness of the unit's infill after the crater's formation. We selected a partially buried impact crater with a diameter of approximately 29 km (center coordinates: 19.48°N, 107.31°E). The present-day height difference between the crater rim and the surrounding plains is about 100 m (Figure 9b). Based on the study by Garvin et al. (2003), we used the following equation to estimate the rim height:

$$hr = 0.02D^{0.84}$$

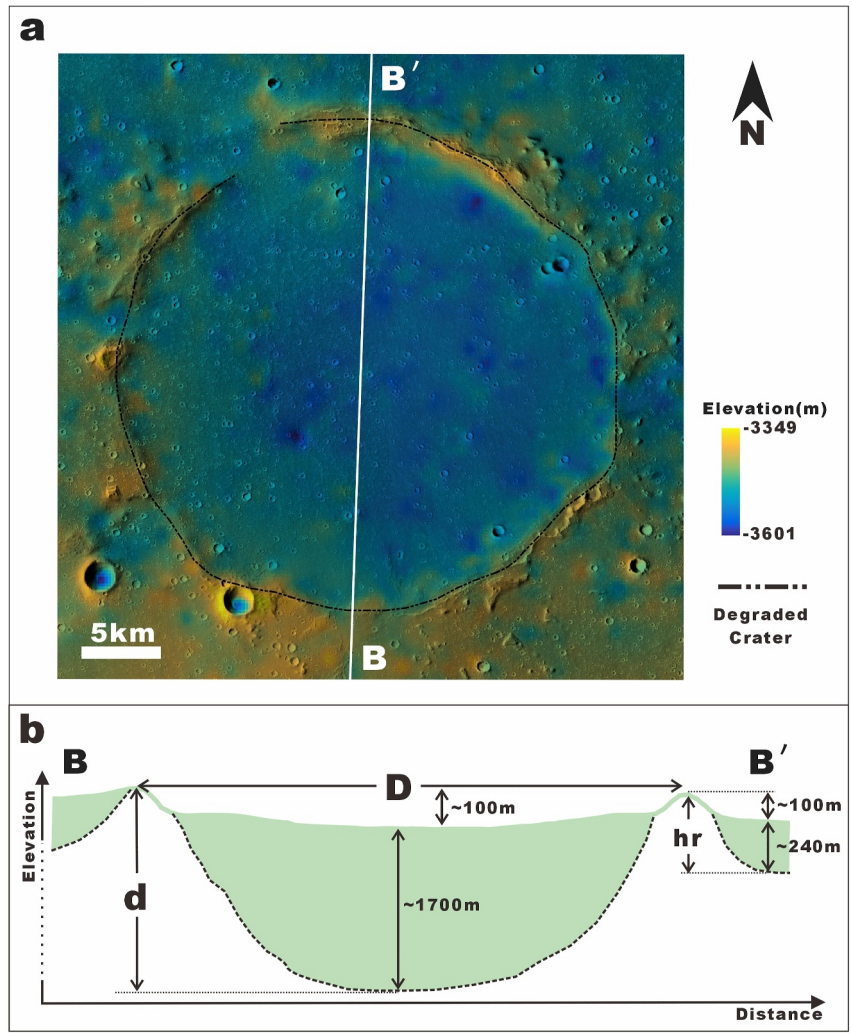

Figure 9. Schematic diagram of the thickness calculation for Hul_1. (a) A diagram illustrating the relationship between the topography profile and impact craters, with the base map being MOLA elevation data overlaid on CTX data, centered at coordinates (19.48°N, 107.31°E). (b) A schematic representation of the theoretical thickness of Hul_1, where the horizontal axis represents distance and the vertical axis represents elevation. A dashed line is for the vertical axis to indicate that this image is not proportionally scaled in the vertical direction to emphasize depth relationships.

where "hr" is the height of the fresh crater rim relative to the surface it was formed in, and "D" is the crater diameter (Figure 9b). The derived original rim height hr is ~340 m, while the present rim height that can be measured is ~100 m. Therefore, we estimate that the local thickness of Hul_1 surrounding the crater is ~240 m.

Boyce and Garbeil (2007) conducted morphological studies on craters of different diameters and derived the relationship between the diameter (D) and depth (d) of craters as follows:

$$d = 0.315D^{0.52} \ (12 \leq D \leq 49\,\text{km})$$

The calculated theoretical depth is about 1,800 m, so the maximum thickness of fill in the impact crater is 1,700 m. This indicates that the Hul_1 unit is ~240 m thick outside the crater but fills the crater itself with a ~1,700 m thick deposit (Figure 9b).

$AHul_2$—Lowland unit 2—This lowland unit is one of the main geological units in the Utopia Planitia region (Figure 8), situated in the northern part of the map and occupying approximately one-third of the total mapping area. In 2021, China's Tianwen-1 landed in the center of this area. The northern part of the unit features numerous

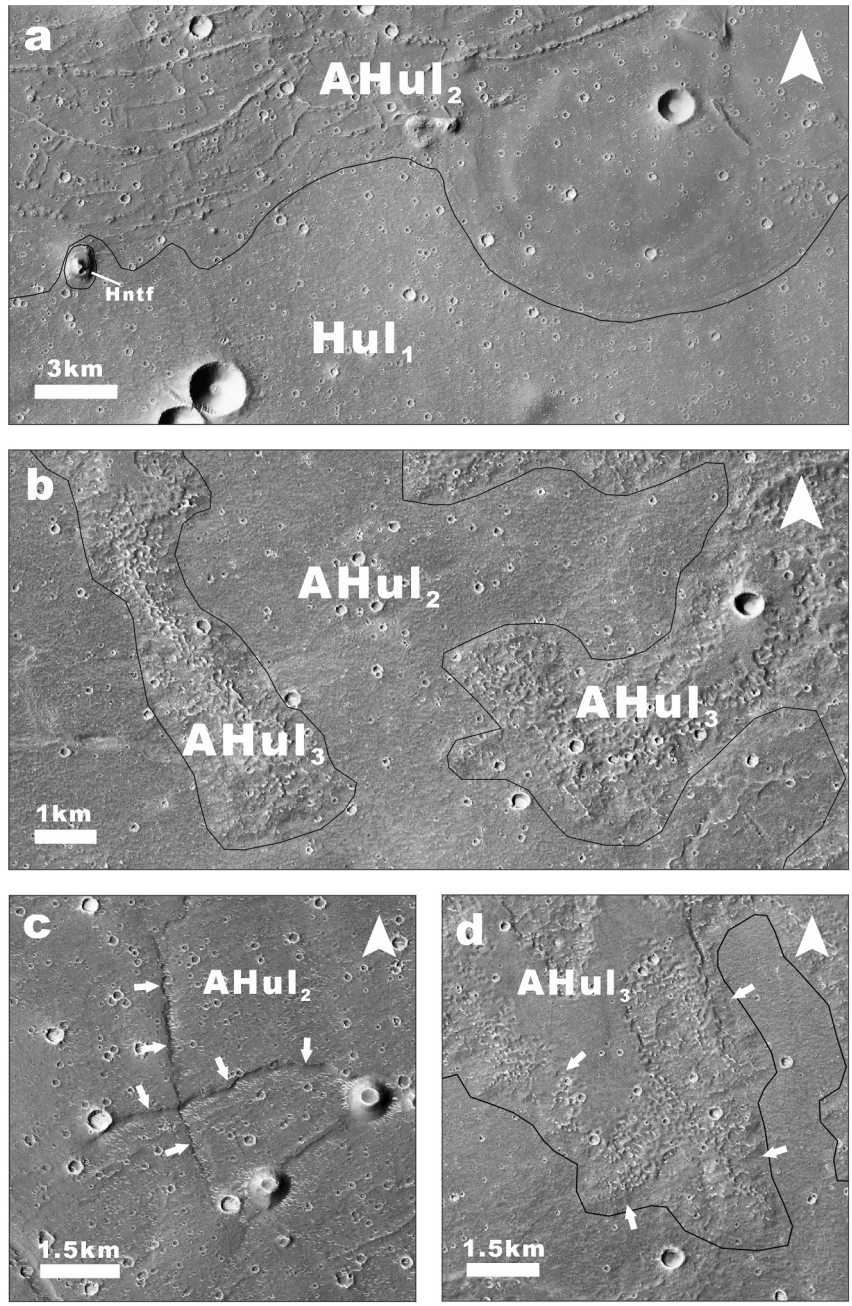

Figure 10. (a) The boundary between $AHul_2$ and Hul_1 with the central coordinates at 20.40°N and 110.25°E. (b) The boundary between $AHul_3$ and $AHul_2$ with the central coordinates at 28.89°N, 107.82°E. (c) Cliffs within the $AHul_2$ unit of Utopia Planitia with the central coordinates at 24.29°N, 111.56°E. (d) Depressions at the edge of the $AHul_3$ unit with the central coordinates at 28.74°N, 108.14°E. The base maps of (a)–(d) are the CTX global mosaic.

polygonal terrain depressions, with the ghost craters (Buczkowski & Cooke, 2004) ranging from 3.5 to 22 km in diameter widely distributed throughout the region. The central and southern parts have many pitted cones and a few mesas that are mapped as unit Hntf within unit $AHul_2$, while the pitted cones in the southern part are aligned as chains. In some locations, Utopia Lowland Unit 2 ($AHul_2$) can be observed overlaying the southern Hul_1 (Figure 10a). In some places, steep cliffs formed by faults or collapses can be observed (Figure 10c). In THEMIS IR daytime images, this area appears relatively bright, indicating that the material has a relatively smaller particle size, with a clear boundary from the southern Hul_1. The surface is relatively smooth with no significant

undulations. There are many fresh, high-albedo impact craters whose ejecta exhibit high thermal inertia characteristics in THEMIS data.

Interpretation: We interpret this unit as Hesperian water-bearing sediments related to outflow channels outside our mapping area.

This unit corresponds to the Vastitas Borealis interior unit (ABvi) as mapped by Tanaka et al. (2005) and Tanaka, Skinner, et al. (2014). It is interpreted as consisting of Hesperian outflow channel deposits, incorporating materials sourced from both the highlands and lowlands, and subsequently modified during the Early Amazonian by the volatilization of internal constituents (Tanaka et al., 2005). According to the chronological study by Skinner and Tanaka (2018), it formed during the Late Hesperian to Early Amazonian. In the global geological map (Tanaka, Skinner, et al., 2014), it corresponds to the Late Hesperian lowland unit. The absolute model age determined in this study is ∼3.59 Ga, consistent with the ∼3.6 Ga age reported by Ivanov et al. (2014).

Many scientists have studied this area, and multiple pieces of evidence suggest that it is related to the water bodies that may have once been widespread in the northern part of Mars, such as the polygonal terrain in the northern part of the unit (Buczkowski et al., 2012; Hiesinger & Head, 2000; McGill & Hills, 1992). Salvatore and Christensen (2014) observed similar phenomena in the Chryse and Acidalia Planum. These similar phenomena have attracted the attention of scientists who concluded that a muddy subsurface unit compacted by sedimentation best explains the features of Utopia Planitia (Buczkowski et al., 2012; Hiesinger & Head, 2000; Ivanov et al., 2014). Additionally, Ivanov et al. (2014) interpreted the widespread etched flows—mud-volcanic deposits that erupted through the VBF—as evidence of a volatile-rich water/ice reservoir beneath central Utopia Planitia during the Late Hesperian.

The pitted cones in the central and southern parts of the region are morphologically similar to terrestrial mud volcanoes or pingos. Wang et al. (2023), after excluding alternative origins such as ice-related cones (e.g., pingos) and rootless cones, concluded that these features represent explosive mud volcanoes. This interpretation implies that subsurface magmatic activity or localized tectonic processes may have driven the eruption of overpressurized sediments. The mesas distributed in this area may also result from the erosion of sediments after the retreat of water bodies (Zhang et al., 2023). The material in this area may originate from sediments deposited by a briefly expanded ancient ocean during the Hesperian, associated with outflow channel activity (e.g., Ivanov et al., 2014; Skinner & Tanaka, 2018; Tanaka et al., 2005; Tanaka, Skinner, et al., 2014). Meanwhile, scientists using data from the Zhurong rover have discovered marine sedimentary rocks formed in a marine environment (Xiao et al., 2023). This may have been due to ancient climatic changes.

Under THEMIS data, a large number of impact craters with high thermal inertia are observed in the region. On the one hand, this suggests that the area has not experienced intense erosion since its formation, allowing the craters to be preserved. On the other hand, the relatively high proportion of fresh craters also indicates that this unit is relatively young.

We therefore interpret this unit as sedimentary deposits emplaced by Hesperian outflow channels (Ivanov et al., 2014; Skinner & Tanaka, 2018; Tanaka et al., 2005; Tanaka, Skinner, et al., 2014) with subsequent modification during the Amazonian period.

$AHul_3$—Lowland unit 3—This unit is located near the central region of Utopia Planitia, covering the northern part of the mapping area. A distinguishing feature of this unit is the presence of numerous small, densely packed depressions—up to ∼400 m in diameter—along its lobate margins (Figure 10b). Near the center of this unit, the development of depressions is not obvious, presenting a flat plateau-like area. However, if some edge areas have severely degraded depressions, the boundary with the surrounding units becomes less distinct, lacking changes in slope. The planar distribution shows some flow characteristics, specifically in the form of fan-shaped sections. Within the unit, there are distinct features such as cracks and polygonal terrain. It is slightly higher than the surrounding units, with an average elevation difference of about 20–30 m. The depressions are not prominent in THEMIS data but are clearly visible in CTX imagery, showing densely developed depressions along the edges.

Interpretation: We interpret this unit to have been formed as a result of the upwelling of underground mud, dating from the Late Hesperian to the Early Amazonian.

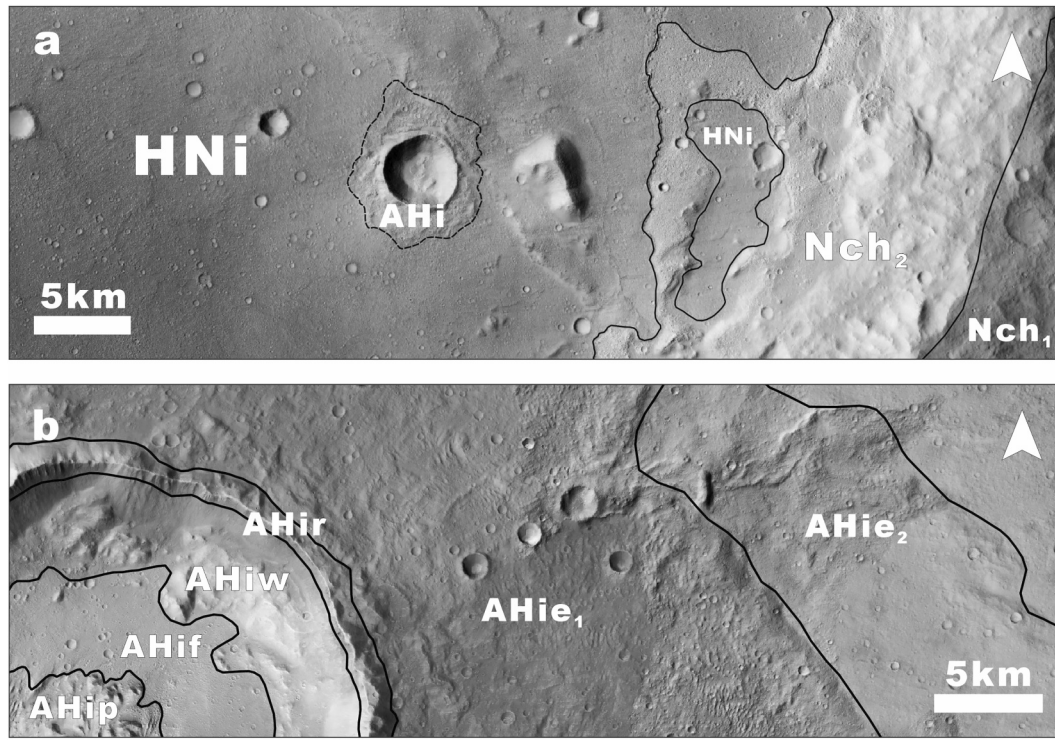

Figure 11. This figure shows the boundaries of the impact crater structures within the mapping area. (a) The boundary of HNi with the surrounding units, with the central coordinates at 6.79°N, 107.01°E; (b) The boundary relationships between different units within the AHi impact crater, with the central coordinates at 12.24°N and 113.43°E.

Ivanov et al. (2014) studied such landforms within Utopia Planitia and defined them as etched flows formed during the Hesperian epoch due to the vertical pressure forcing underground mud to erupt onto the surface.

The distribution of Utopia Lowland Unit 3 ($AHul_3$) coincides with the polygonal terrain (Figure A1). The formation of the polygonal terrain may have provided pathways for mud to migrate from the subsurface to the surface (Ivanov et al., 2014). Therefore, it is possible that $AHul_3$ formed simultaneously with the polygonal terrain. $AHul_3$ overlies $AHul_2$, indicating that its final emplacement occurred after ~3.59 Ga, likely during the Early Amazonian.

From a morphological perspective, $AHul_3$ differs from typical lava flows, with its edges featuring numerous depressions, indicating weaker erosion resistance. Indeed, the materials of $AHul_3$ are of relatively fine-grained materials interpreted from THEMIS IR nighttime data. Cuřín et al. (2023) also studied similar landforms in Adamas Labyrinthus, southwest of Utopia Planitia, and proposed that the upwelling mud formed an ice crust upon freezing at the surface. The mud overflowed from the edges of the ice crust, and the subsequent volatilization or sublimation created the lobate edges filled with depressions.

We interpret this unit as mud-derived deposits, potentially linked to the presence of water bodies in central Utopia Planitia (Cuřín et al., 2023; Ivanov et al., 2014).

4.5. Impact Crater Units

HNi—Impact Crater material, degraded—Degraded impact craters in the southern highlands of Terra Cimmeria, characterized by the absence of well-preserved crater rims and ejecta deposits. Most of the craters have a circular shape and are filled with other materials, forming a flat crater floor. The crater walls show slumping toward the central area (Figure 11).

Interpretation: The ancient impact craters are heavily degraded and filled with other materials. According to Mangold et al. (2012), impact craters lacking observable central peaks and ejecta are classified as Type I in their system, with formation predominantly occurring prior to ~3.7 Ga. Following its formation, the HNi unit

underwent degradation through two concurrent processes: (a) structural collapse and mass wasting associated with magma withdrawal events that led to the formation of the Nch_2 and Nch_3 units around ~3.89 Ga, and (b) hydrodynamic scouring by contemporaneous meltwater outflows (Figure 5c), which further eroded the unit. Around ~3.46 Ga, subsequent small-scale extrusion activity infilled these ancient craters, and wrinkle ridges formed as a result of tectonic compression during lava cooling. Subsequently, they continued to be filled with other materials, such as ejecta from younger surrounding impact craters and lava from deep faults in the impact craters, consistent with the intrusive intrusion model proposed by Jozwiak et al. (2012).

AHi—Impact Crater material, preserved—Impact crater materials are distributed throughout the study area, preserving relatively complete impact crater structures (Figure 11a). In some larger impact craters, more detailed impact structures can be identified (Figure 11b).

Interpretation: Impact-related materials are distributed across various units in the mapped area. Such impact craters typically exhibit well-preserved central peaks and ejecta. According to the research by Mangold et al. (2012), these craters are classified as Type II and III, with their formation predominantly occurring during the Hesperian and Amazonian periods. AHi units are distributed throughout the mapping area, with the largest example measuring approximately 55 km in diameter, centered at 12°N, 105°E. Morphological variations are observed among AHi craters at different locations. For instance, those in the central part of the mapping area commonly display double-layered ejecta, while craters in the northern region exhibit single-layered, pancake-like, or rampart morphologies (Ivanov et al., 2014). These differences are likely attributable to spatial variations in target material composition.

AHip—Impact crater peak located at the center of the AHi unit is characterized by a mound- or cone-shaped central uplift with a rough, brecciated surface texture (Figure 11b).

Interpretation: Formed by elastic rebound of deep target rocks during the modification stage of the impact, intense fracturing and hydrothermal alteration leave a blocky texture (Melosh, 1989; Osinski & Pierazzo, 2012). Minor coatings of impact melt or fallback breccia may contribute to additional surface roughness.

AHif—Impact crater floor, the flat area in the central region of the impact crater (Figure 11b), has a local distribution of numerous sand dunes.

Interpretation: A coherent impact melt sheet was emplaced, cooled, and leveled, followed by isostatic settling (Grieve & Cintala, 1992; Osinski & Pierazzo, 2012). Subsequent deposition of thin layers of sediment, lava, or aeolian dust further smoothed any residual topographic relief.

AHiw—Impact crater wall, the steep inner wall of the impact crater (Figure 11b), near the edge and closer to the center, showing terraces and slump scars.

Interpretation: Rotational slumping along listric faults leads to the development of multi-terraced crater walls. Continued mass wasting, potentially aided by the melting of ice-rich layers, further enhances wall collapse (Kenkmann et al., 2014; Melosh, 1989).

AHir—Impact crater rim, the circular ring protruding above the surface (Figure 11b), crest discontinuous.

Interpretation: Uplifted and overturned strata, mixed with proximal ejecta during the excavation stage, form the crater rim. Subsequent aeolian abrasion and secondary impacts contribute to rim notching and breaching (Melosh, 1989).

$AHie_1$—Impact crater ejecta 1 (inner), the proximal ejecta of the impact crater (Figure 11b), rough, lobate, high-thermal-inertia deposit immediately outside the rim.

Interpretation: Coarse, melt-rich ballistic ejecta were emplaced during the initial collapse of the ejecta curtain, commonly containing impact melt veneers and blocky breccias (Barnouin-Jha & Schultz, 1998; Osinski et al., 2005).

$AHie_2$—Impact crater ejecta 2 (outer), the ejecta near the outer side of the impact crater (Figure 11b), smoother blanket with radial grooves and secondary pits.

Table 1
Information From Geological Maps Compiled by Different Scholars

Author	Year	Geologic map	Scale	Database
Hiller	1979	Geologic Map of the Amenthes Quadrangle of Mars (I-1110)	1:5,000,000	Mariner 9
Tanaka et al.	2014	Geologic Map of Mars (SIM-3292)	1:20,000,000	MOLA DEM; THEMIS
Skinner and Tanaka	2018	Geologic Map of the Nepenthes Planum Region, Mars	1:1,500,000	MOLA DEM; THEMIS; CTX; HiRISE

Interpretation: Fine-grained distal ejecta were deposited from the later, decelerating phase of the ejecta curtain. Radial lineations and secondary craters reflect velocity decay and ballistic clustering during emplacement (Barnouin-Jha & Schultz, 1998; Schultz & Gault, 1979).

5. Discussion

5.1. Comparison to Previous Maps

Previous studies have conducted varying degrees of mapping work on the entire or parts of the study area, with scales ranging from 1:20,000,000 to 1:1,500,000 (Erkeling et al., 2011; Hiller, 1979; Ivanov et al., 2014; Skinner & Tanaka, 2018; Tanaka, Skinner, et al., 2014). These studies utilized data sets from Mariner 9, MOLA, THEMIS daytime and nighttime data, and CTX, among others (Table 1).

Compared to the aforementioned geological maps, we have used a larger scale (1:1,000,000 for digital mapping). This allowed us to delineate more detailed geological units and identify different geological units in the Terra Cimmeria and Amenthes regions. With the support of CTX and other data, the boundaries of each unit are more accurately defined. Compared to Skinner and Tanaka (2018), our geological map covers a larger north-south range, adding units $AHul_3$, Hap, Nat, and HNaf.

Ivanov et al. (2014) conducted a geomorphologic analysis of the southwestern portion of Utopia Planitia and mapped the etched flow as the "Etched flows" unit. We have delineated the etched flow as the $AHul_3$ unit and identified its boundaries more accurately using CTX high-resolution images, better illustrating its position within the mapped area and its relationship with other geological features.

Erkeling et al. (2011) conducted morphological and stratigraphic investigations of the Amenthes region, producing a series of geological maps and stratigraphic correlation charts, providing a good chronological analysis of Amenthes Planum and Amenthes Fossae. Based on our digital mapping with 1:1,000,000 scale, we have updated our understanding of Amenthes Fossae. We agree that this unit formed during the Noachian period (Erkeling et al., 2011), but through the cross-cutting relationships between different units (Figures 2b and 2c), we have discovered that this geological unit formed two grabens approximately 3.71 Ga ago, demonstrating complex tectonic activity.

Compared to previous geological maps that cover a wide area, we provide higher resolution boundaries of geological units. In contrast to SIM 3389, our map covers approximately 25° of latitude and includes multiple geological units ranging from the Noachian to the Amazonian periods. Additionally, we have provided new insights into the formation and evolution timeline of Amenthes Fossae.

5.2. Geologic History

Based on our detailed geological mapping, we interpret the geological history as follows:

5.2.1. Late Noachian Erosion of the Glaciated Highland

In the geological map, Terra Cimmeria is interpreted as an Early Noachian terrain (Tanaka, Skinner, et al., 2014) composed of ancient impact breccias that predate the formation of Utopia Planitia (Skinner & Tanaka, 2018). This region was designated as the Nch_1 unit in our mapping. During the Late Noachian period (Figure 14), the southern highlands preserved a significant amount of ice. Extensive extrusion activity led to the melting of this ice and subsequent erosion of the landscape (Head & Wilson, 2007). The eroded areas formed Nch_2 and Nch_3, while the part near Amenthes Planum was eroded to form Nat (Figure 2a). After the lava cooled, multiple wrinkle ridges

developed (Watters, 1988) on the Nch_3 unit (Figure 5b). The widespread extrusive activity likely caused a brief temperature increase in the region, releasing meltwater (Halevy & Head, 2014). Channels developed on Nat, which later evolved into inverted channels (Williams et al., 2009) (Figure 5c). The surface or near-surface ice that may have formed during the Late Noachian (Fastook & Head, 2015) in Nch_1 began to melt, forming meltwater channels (Figure 4c).

5.2.2. Early Hesperian Multi-Regional Extrusive Activity

During the Early Hesperian period (Figure 14), the region experienced a second phase of extensive extrusive activity. The Nepenthes transitional flow unit (Hntf) is likely formed by the combined action of erupting lava flows and mudflows (Tanaka, Carr, et al., 2003). As the lava flows cooled, numerous north-south oriented wrinkle ridges were formed (Figure 7c). Consequently, the volatilization of water or ice led to the development of rough surface texture (Figure 7a). Near the northern boundary of the Hntf unit, there are several tuff cones formed as a result of interactions between magma and subsurface water (Brož & Hauber, 2013). This unit may extend further north, covering Utopia Planitia and forming its underlying wrinkle ridge plains (Figure 13). At approximately 3.71 Ga, the region experienced extensional stress, leading to the development of Amenthes Fossae, which cut through Nch_2, Nch_3, and Nat (Figures 2b and 2c). The Amenthes Fossae cuts through the Hntf unit while being overlain by it.

Similarly, during the Early Hesperian, active extrusive activity in the southwestern mapping area led to large volumes of lava flowing in and filling the Amenthes Planum, covering the weathered sediments from the Noachian period (Erkeling et al., 2011). This also covered parts of the Amenthes transitional unit (Nat) and Amenthes Fossae unit (HNaf) (Figure 2b). During the subsequent tectonic compression by the cooling of lava, many wrinkle ridges developed, and the streamlined grooves on the surface may have been formed by water or lava flow.

During the ~3.66 Ga, small-scale extrusion and water activity erosion occurred in the southern highlands. Some low-lying areas may have temporarily accumulated high-salinity brines, forming polygonal ridges as the water sublimated (Figure 5d).

Around 3.46 billion years ago, during the Early Hesperian, extrusive activity occurred within ancient impact craters, and the faults at the base of the impact craters may have provided access to magma (Jozwiak et al., 2012). The crater floors were filled with lava, and the crater walls experienced modification (Figure 11a). Wrinkle ridges formed on the crater floors.

5.2.3. Formation of the Amenthes Cavi

During the Hesperian period (Figure 14), the area north of Amenthes Cavi experienced extensive material infill and coverage, burying numerous impact craters and mesas (Figure 7d). The sharp edges of many partially buried impact craters remain well-preserved.

In our mapping area, Amenthes Cavi presents irregular depressions with arcuate boundaries, which are predominantly located at the contact between the Hntf and Hul_1 units (Figure 12). The interior slopes of these depressions are gentle.

There are different hypotheses regarding the origin of Amenthes Cavi. Skinner and Tanaka (2007) attributed it to collapse following mud reservoir depletion at depth. Another possibility is that changes in Mars' axial tilt (Montmessin, 2007) led to the melting of subsurface ice, which in turn formed Amenthes Cavi. However, if this were the case, the distribution of Amenthes Cavi should follow a latitudinal pattern rather than being concentrated in the northern part of the Hntf unit. Based on the research about the depressions near the etched flows, Ivanov et al. (2014) suggested that the release of subsurface fluids may have caused the collapse of strata and surface subsidence. In our study, the area containing Amenthes Cavi also hosts tuff cones interpreted to be associated with intrusive activity, indicating the presence of subsurface magmatic processes. Consequently, the formation of Amenthes Cavi likely involved contributions from subsurface intrusion. Therefore, we believe that during the Hesperian, underground intrusive activity in the Amenthes Cavi and northern regions caused the melting of the permafrost layer, the release of subsurface fluids led to the collapse of the strata (Wilson & Head, 2004). The resulting debris flows developed northward, burying the mesas and impact craters (Figure 7d). Due to the

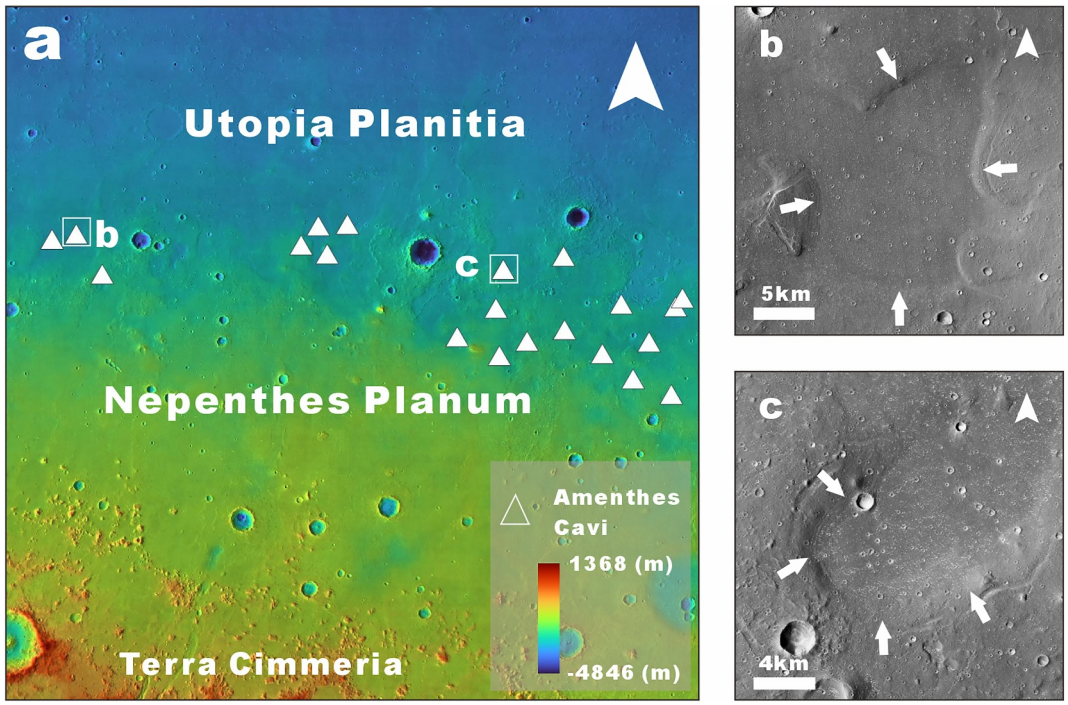

Figure 12. (a) The location of Amenthes Cavi within the mapping area, with a central coordinate of 15.0°N, 110.0°E and the basemap is MOLA DEM overlay on the MoRIC. (b) An Amenthes Cavi located on the western side, with a central coordinate of 17.86°N, 106.07°E and a base map of CTX global mosaic. (c) An Amenthes Cavi located in the central region, with a central coordinate of 17.35°N, 112.13°E and a base map of CTX global mosaic.

northward loss of material, the Amenthes Cavi area saw the formation of numerous depressions caused by terrain collapse. This unit may extend into the interior of the Utopia Basin, but the exact boundaries are still unclear (Figure 13).

5.2.4. Formation of the Vastitas Borealis Formation

From the Late Hesperian to the Early Amazonian period (Figure 14), the formation and evolution of the VBF were the main geological event for the $AHul_2$. Due to the development of outflow channels during the Hesperian

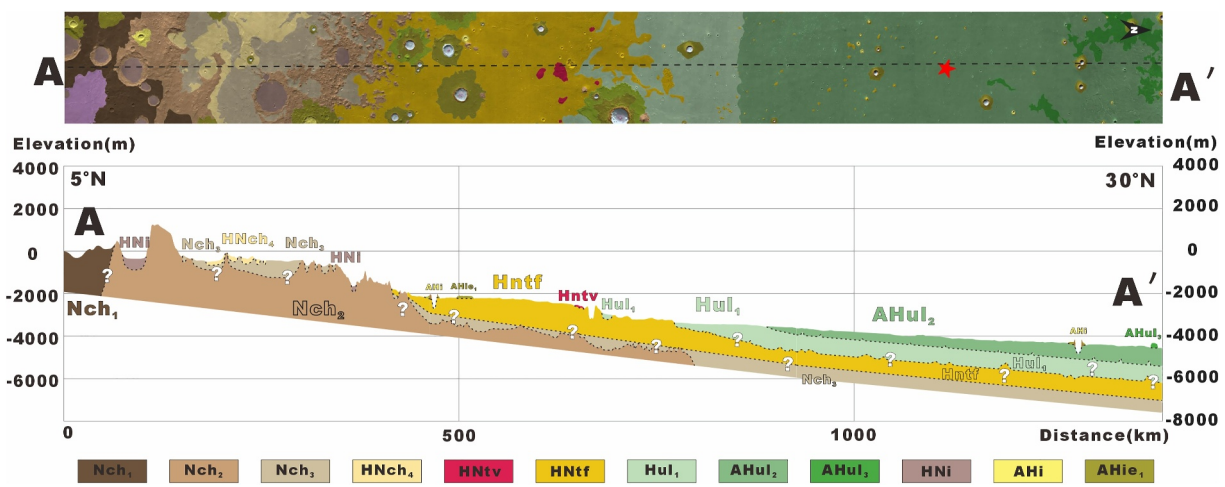

Figure 13. Schematic diagram of the stratigraphic profile. The dashed lines and question marks represent the inferred relationships of the underground strata. The Noachian units in the southern part of the mapping area exhibit rugged surfaces, with some being overlaid by younger units. The Hntf unit in the central part may have extended further to the north, but it was later covered by other units. The lower layers of the Utopia Planitia in the northern part may contain highland materials from the Noachian and Hesperian epochs.

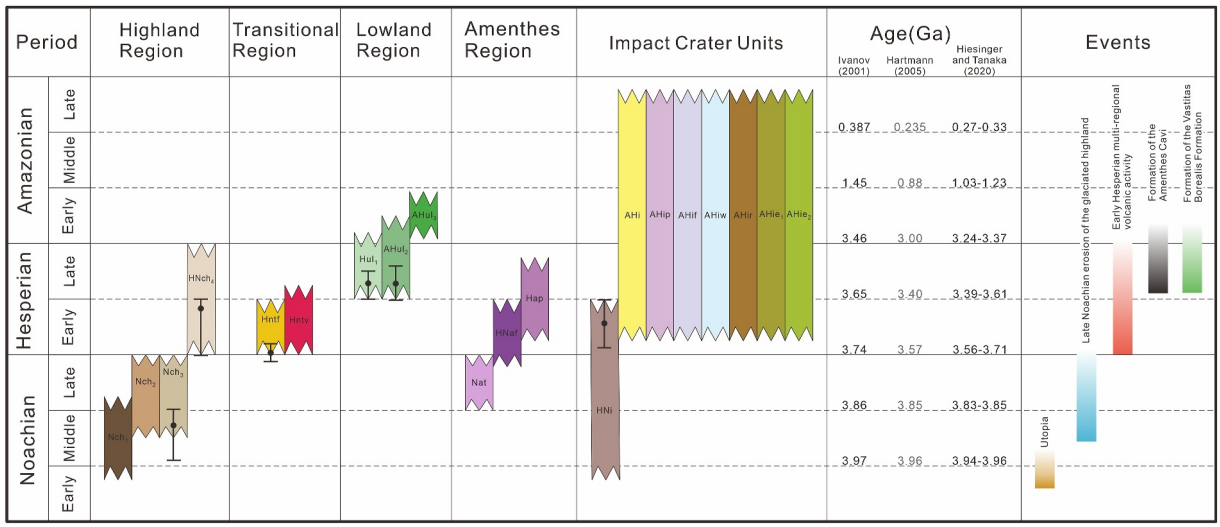

Figure 14. Stratigraphic column chart. The sawtooth pattern represents the estimated approximate start and end times. Most geological units were formed during the Late Noachian to Early Amazonian epochs. The units of the Highland Region predominantly formed during the Noachian, whereas the units of the Transitional Region were mainly formed during the Early Hesperian. The units of the Lowland Region primarily formed during the Late Hesperian to Early Amazonian epochs, and the units of the Amenthes Region predominantly formed from the Late Noachian to the Late Hesperian epochs.

period, large amounts of water-laden sediments flowed into the northern lowlands (Baker et al., 1991; Parker et al., 1989, 1993; Tanaka, 1997), including Utopia Planitia (Ivanov et al., 2014). The influx of the VBF covered the Hntf, an extrusive unit, aligning vertically with Zhao et al. (2021)'s stratigraphic division of Utopia Planitia, where the VBF lies above the wrinkle ridge plains.

In the northern part of the mapping area, within Utopia Planitia, polygonal terrains (Figure 8) and fractures appeared, likely due to the pressure from overlying strata causing fracturing and subsidence (Ivanov et al., 2014). Under vertical stratigraphic pressure, deep mud began to rise along these fractures and erupted from surface cracks (Ivanov et al., 2014). Due to the low temperatures, the initially erupted mud formed an ice crust on the outside, with subsequent mud flows emerging from beneath this ice crust. The edges of the mudflows developed numerous depressions due to the volatilization and sublimation of water (Cuřín et al., 2023). The various degradation states of these etched flows suggest that the mud upwelling process was episodic, accompanying the subsidence of the strata. Additionally, due to intermittent underground intrusive activity, small units such as pitted cones (Komatsu et al., 2011; Wang et al., 2023) in the southern part of the VBF.

6. Discussion About the Potential Landing Area of Tianwen-3 Mars Sample Return Mission

The primary objective of the Tianwen-3 mission is to search for signs of life on Mars. Based on both scientific priorities and engineering constraints (Table 2), the landing site must be selected within defined parameters to ensure a safe descent and landing (Hou et al., 2024). The Tianwen-3 science team has proposed 86 potential landing sites, two of which are located within Utopia Planitia (Hou et al., 2024).

Table 2
Engineering Constraints for the Tianwen-3 Mission (Hou et al., 2024)

Parameters	Value
Altitudes	≤−3 km
Latitudes	17°–30°N
Slopes	≤8°
Rock abundances	≤10%

The $AHul_2$ unit is the largest geomorphological unit within the mapped region of Utopia Planitia and displays a variety of landforms indicative of past water or ice-related processes. We interpret the $AHul_2$ unit as comprising VBF materials emplaced by Hesperian outflow channels. The VBF extends across much of the northern lowlands, including Utopia Planitia. Numerous landforms—including mud volcanoes (Wang et al., 2023), mudflows (Cuřín et al., 2023), giant polygons (Hiesinger & Head, 2000), and circular grabens (Buczkowski et al., 2012)—support the sedimentary origin of the VBF and the potential existence of an ancient northern ocean (Ivanov et al., 2014; Wang & Huang, 2024).

The Zhurong rover landed in the southern part of Utopia Planitia in May 2021, within the VBF unit. Observations from the Multispectral Camera (MSCam) identified rocks with bedding and inclined stratification; by comparing these structures to terrestrial analogs formed in various environments, Xiao et al. (2023) ruled out aeolian origins and interpreted the features as indicative of deposition in a shallow marine setting. Subsurface radar data from the low-frequency channel of the Rover-mounted Subsurface Penetrating Radar (RoPeR) revealed two sets of normally graded subsurface layers, interpreted by C. Li et al. (2022) as products of episodic catastrophic flooding events during the Late Hesperian to Early Amazonian. Further analysis by J. Li et al. (2025) imaged multilayered sedimentary reflectors dipping unidirectionally at 6°–20°, located 15–35 m below the surface along a 1.3 km traverse perpendicular to a proposed paleo-shoreline, and interpreted them as coastal deposits. These multiple lines of evidence for aqueous processes underscore the $AHul_2$ unit's potential for preserving biosignatures.

Based on the experience of Wu et al. (2022) in defining landing ellipses for the Tianwen-1 mission, the potential landing ellipse dimensions were approximately 56 km along the long axis and 22 km along the short axis. This standard may serve as a reference framework for delineating the landing area of the Tianwen-3 mission.

7. Conclusion

Our 1:1,000,000-scale geological mapping and stratigraphic analysis of southern Utopia Planitia (5°–30°N, 105°–115°E) near the Martian dichotomy boundary has provided refined insights into the geologic history and crustal evolution of this transitional region. Key findings are summarized as follows:

1. We identified 20 distinct geological units and classified them into five major groups: four highland units ($HNch_4$, Nch_3, Nch_2, Nch_1), two transitional units (Hntf, Hntv), three lowland units ($AHul_3$, $AHul_2$, Hul_1), three Amenthes region units (Nat, Hap, HNaf), and eight impact-related units (HNi, AHi, AHip, AHif, AHiw, AHir, $AHie_1$, $AHie_2$). These units collectively record stratigraphic assemblages spanning from the Early Noachian to the Early Amazonian, capturing key transitions in regional tectonic, volcanic, and hydrologic processes.
2. CSFD analyses, combined with cross-cutting and superpositional relationships, allow the subdivision of the regional geological history into five stages. These include two large-scale extrusive episodes during the Late Noachian and Early Hesperian, two regional extrusive events related to the development of wrinkle ridge plains and tuff cones, and one intrusive event that drove volatile loss and sediment mobilization in the Hesperian.
3. The Hul_1 unit, interpreted as a Hesperian debris flow deposit at the southern margin of Utopia Planitia, has a maximum surface thickness of ∼240 m, calculated based on the burial depth of a partially infilled 29-km-diameter impact crater. Infill thickness within the crater itself reaches ∼1,700 m, implying substantial sediment accumulation following formation of the crater.
4. The $AHul_2$ unit, occupying the northern part of the map and corresponding to the VBF, is composed of Hesperian to Amazonian outflow channel deposits. It meets all engineering constraints for China's Tianwen-3 sample return mission (altitude ≤ -3 km, latitude 17°–30°N, slope $\leq$8°, rock abundance $\leq$10%) and preserves abundant evidence for past aqueous processes, including polygonal terrain, pitted cones, and potential mud volcanoes. $AHul_2$ is thus identified as a scientifically compelling and technically viable landing candidate.

These findings offer an updated geologic framework for interpreting the tectono-thermal and aqueous history of the Martian dichotomy boundary in southern Utopia Planitia, with important implications for understanding Mars' ancient climate and informing future exploration strategies.

Appendix A

Geologic map of the dichotomy region in the southern Utopia Planitia, Mars and model ages of selected geologic units, derived using the Ivanov (2001) production function and the Hartmann and Neukum (2001) chronology function.

Figure A1

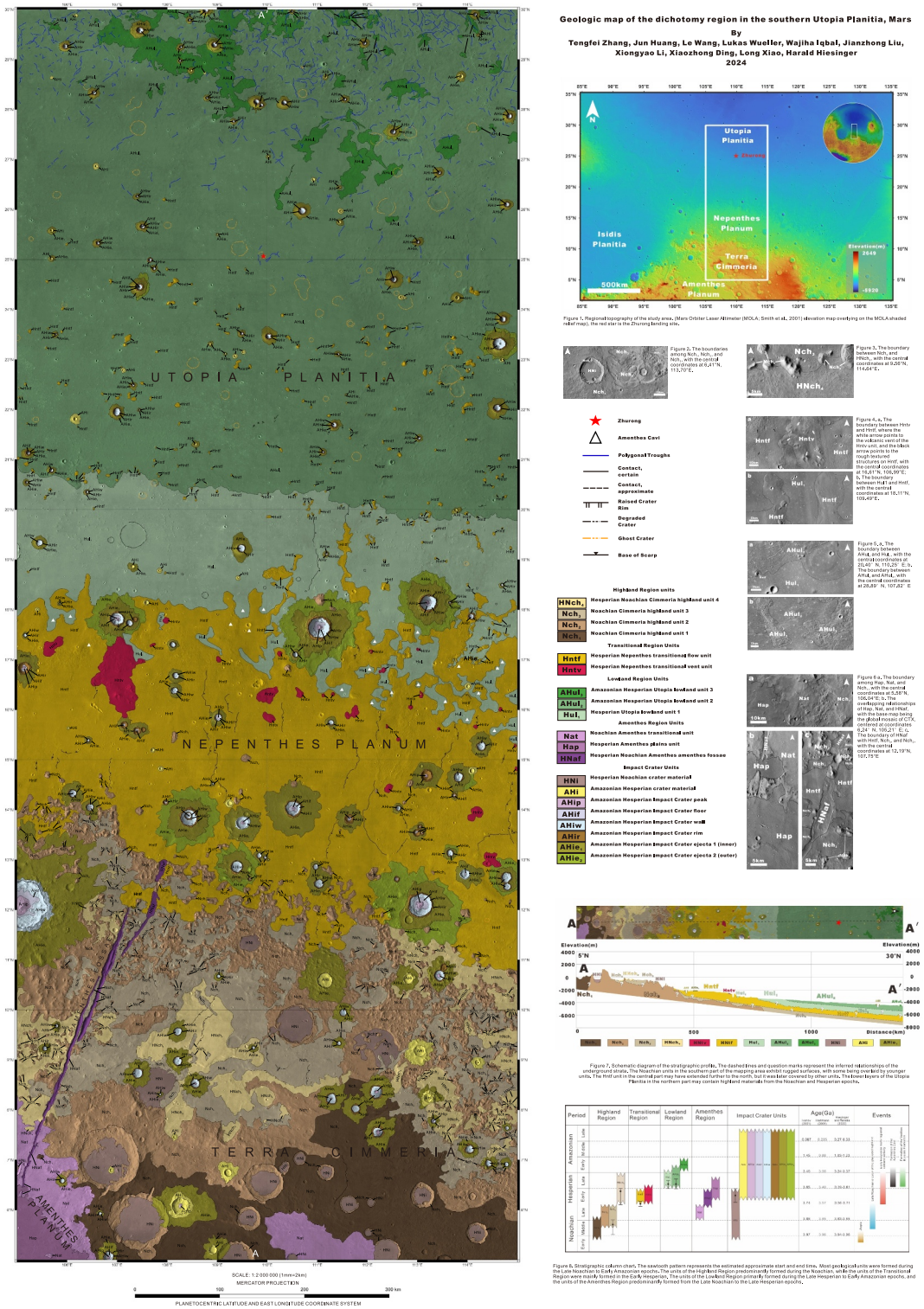

Figure A1. Geologic map of the dichotomy region in the southern Utopia Planitia, Mars. This map shows the distribution of different geologic units within the mapping area, highlighted by color coding. The included figures illustrate the details of various geological units and their interrelationships.

Figure A2

Unit name	Area (/km²)	(N)1 (/km²)	Neukum-Ivanov 2001 (Ga)
$AHul_2$	8230	0.00384	$3.59^{+0.070}_{-0.140}$
Hul_1	2850	0.00441	$3.63^{+0.086}_{-0.22}$
Hntf	4100	0.00666	$3.71^{+0.047}_{-0.070}$
$HNch_4$	775	0.00505	$3.66^{+0.090}_{-0.27}$
Nch_3	880	0.0182	$3.89^{+0.058}_{-0.098}$
HNi	530	0.00251	$3.46^{+0.045}_{-0.063}$

Figure A2. Model ages of selected geologic units were derived using the Ivanov (2001) production function and Hartmann and Neukum (2001) chronology function. The count areas were confined to individual geological units and were sufficiently large to ensure statistical reliability. Crater diameters were measured in QGIS using the OpenCraterTool plugin (Heyer et al., 2023), with efforts made to exclude secondary crater chains and clusters.

Data Availability Statement

The final geologic map and related CSFD files are available via Zenodo (Zhang et al., 2025). THEMIS IR data (Christensen et al., 2004), HiRISE images (McEwen et al., 2007), and HRSC-MOLA blended DEM (Fergason et al., 2018) are available from the PDS. The CTX global mosaic data are available at the Caltech Murray Lab (Dickson et al., 2018) and are archived in the PDS. The MoRIC data (Liu et al., 2024) used in this work was processed and produced by the Ground Research and Application System (GRAS) of China's Lunar and Planetary Exploration Program.

Acknowledgments
This work was supported by the National Key R&D Program of China (Grant 2024YFF0807702) and the National Natural Science Foundation of China (Grants 42441801 and 42273041). The authors thank Dr. Jean-Pierre Williams for editorial handling and appreciate the constructive comments provided by Holly Buban and an anonymous reviewer, which helped improve the clarity and quality of the manuscript.

References

Barnouin-Jha, O. S., & Schultz, P. H. (1998). Lobateness of impact ejecta deposits from atmospheric interactions. *Journal of Geophysical Research*, *103*(E11), 25739–25756. https://doi.org/10.1029/98je02025

Baker, V., Strom, R., Gulick, V., Kargel, J., Komatsu, G., & Kale, V. (1991). Ancient oceans, ice sheets and the hydrological cycle on Mars. *Nature*, *352*(6336), 589–594. https://doi.org/10.1038/352589a0

Boyce, J. M., & Garbeil, H. (2007). Geometric relationships of pristine Martian complex impact craters, and their implications to Mars geologic history. *Geophysical Research Letters*, *34*(16), L16201. https://doi.org/10.1029/2007gl029731

Brož, P., & Hauber, E. (2013). Hydrovolcanic tuff rings and cones as indicators for phreatomagmatic explosive eruptions on Mars. *Journal of Geophysical Research: Planets*, *118*(8), 1656–1675. https://doi.org/10.1002/jgre.20120

Buczkowski, D. L., & Cooke, M. L. (2004). Formation of double-ring circular grabens due to volumetric compaction over buried impact craters: Implications for thickness and nature of cover material in Utopia Planitia, Mars. *Journal of Geophysical Research*, *109*(E2), 2003JE002144. https://doi.org/10.1029/2003JE002144

Buczkowski, D. L., Seelos, K. D., & Cooke, M. L. (2012). Giant polygons and circular graben in western Utopia basin, Mars: Exploring possible formation mechanisms. *Journal of Geophysical Research*, *117*(E8), E08010. https://doi.org/10.1029/2011JE003934

Carr, M. (1996). *Water on Mars*. Oxford University Press.

Carr, M. H. (2007). *The surface of Mars* (Vol. 6). Cambridge University Press. https://doi.org/10.1017/cbo9780511536007

Carr, M. H., & Head, J. W. (2003). Oceans on Mars: An assessment of the observational evidence and possible fate. *Journal of Geophysical Research*, *108*(E5), 5042. https://doi.org/10.1029/2002je001963

Christensen, P. R., Jakosky, B. M., Kieffer, H. H., Malin, M. C., McSween Jr, H. Y., Nealson, K., et al. (2004). The thermal emission imaging system (THEMIS) for the Mars 2001 Odyssey Mission [Dataset]. *Space Science Reviews*, *110*(1/2), 85–130. https://doi.org/10.1023/b:spac.0000021008.16305.94

Chuang, F. C. (2015). Fretted terrain. In H. Hargitai & Á. Kereszturi (Eds.), *Encyclopedia of planetary landforms* (pp. 817–821). Springer New York. https://doi.org/10.1007/978-1-4614-3134-3_410

Clifford, S. M., & Parker, T. J. (2001). The evolution of the Martian hydrosphere: Implications for the fate of a primordial ocean and the current state of the northern plains. *Icarus*, *154*(1), 40–79. https://doi.org/10.1006/icar.2001.6671

Craddock, R. A., & Howard, A. D. (2002). The case for rainfall on a warm, wet early Mars. *Journal of Geophysical Research*, *107*(E11), 21-1–21-36. https://doi.org/10.1029/2001je001505

Cuřín, V., Brož, P., Hauber, E., & Markonis, Y. (2023). Mud flows in southwestern Utopia Planitia, Mars. *Icarus*, *389*, 115266. https://doi.org/10.1016/j.icarus.2022.115266

Dickeson, Z. I., & Davis, J. M. (2020). Martian oceans. *Astronomy & Geophysics*, *61*(3), 3.11–3.17. https://doi.org/10.1093/astrogeo/ataa038

Dickson, J., Kerber, L., Fassett, C., & Ehlmann, B. (2018). A global, blended CTX mosaic of Mars with vectorized seam mapping: A new mosaicking pipeline using principles of non-destructive image editing [Dataset]. In *Lunar and planetary science conference* (Vol. *49*, pp. 1–2). Lunar and Planetary Institute. https://doi.org/10.17189/m23v-ae12

Erkeling, G., Hiesinger, H., Reiss, D., Hielscher, F. J., & Ivanov, M. A. (2011). The stratigraphy of the Amenthes region, Mars: Time limits for the formation of fluvial, volcanic and tectonic landforms. *Icarus*, *215*(1), 128–152. https://doi.org/10.1016/j.icarus.2011.06.041

Fastook, J. L., & Head, J. W. (2015). Glaciation in the Late Noachian Icy Highlands: Ice accumulation, distribution, flow rates, basal melting, and top-down melting rates and patterns. *Planetary and Space Science*, *106*, 82–98. https://doi.org/10.1016/j.pss.2014.11.028

Fergason, R., Hare, T., & Laura, J. (2018). HRSC and MOLA blended digital elevation model at 200m v2, astrogeology PDS annex [Dataset]. *US Geological Survey*. https://astrogeology.usgs.gov/search/map/mars_mgs_mola_mex_hrsc_blended_dem_global_200m

FGDC. (2006). *Fgdc digital cartographic standard for geologic map symbolization*. Citeseer.

Frey, H., & Schultz, R. A. (1988). Large impact basins and the mega-impact origin for the crustal dichotomy on Mars. *Geophysical Research Letters*, *15*(3), 229–232. https://doi.org/10.1029/gl015i003p00229

Frey, H. V., Roark, J. H., Shockey, K. M., Frey, E. L., & Sakimoto, S. E. (2002). Ancient lowlands on Mars. *Geophysical Research Letters*, *29*(10), 22-1–22-4. https://doi.org/10.1029/2001gl013832

Frey, H. V., & Schultz, R. A. (1990). Speculations on the origin and evolution of the Utopia-Elysium lowlands of Mars. *Journal of Geophysical Research*, *95*(B9), 14203–14213. https://doi.org/10.1029/jb095ib09p14203

Garvin, J., Sakimoto, S., & Frawley, J. (2003). Craters on Mars: Global geometric properties from gridded MOLA topography. In *6th International Conference on Mars*. Lunar and Planetary Institute.

Greeley, R., & Guest, J. (1987). Geologic map of the eastern equatorial region of Mars. *Citeseer*, *1*.

Grieve, R. A. F., & Cintala, M. J. (1992). An analysis of differential impact melt-crater scaling and implications for the terrestrial impact record. *Meteoritics*, *27*(5), 526–538. https://doi.org/10.1111/j.1945-5100.1992.tb01074.x

Halevy, I., & Head III, J. W. (2014). Episodic warming of early Mars by punctuated volcanism. *Nature Geoscience*, *7*(12), 865–868. https://doi.org/10.1038/ngeo2293

Hartmann, W. K. (1973). Martian cratering, 4, Mariner 9 initial analysis of cratering chronology. *Journal of Geophysical Research*, *78*(20), 4096–4116. https://doi.org/10.1029/jb078i020p04096

Hartmann, W. K., & Neukum, G. (2001). Cratering chronology and the evolution of Mars. In *Chronology and evolution of Mars: Proceedings of an ISSI Workshop, 10–14 April 2000, Bern, Switzerland* (pp. 165–194). Springer.

Head, J. W., Hiesinger, H., Ivanov, M. A., Kreslavsky, M. A., Pratt, S., & Thomson, B. J. (1999). Possible ancient oceans on Mars: Evidence from Mars Orbiter Laser Altimeter data. *Science*, *286*(5447), 2134–2137. https://doi.org/10.1126/science.286.5447.2134

Head III, J. W., & Wilson, L. (2007). Heat transfer in volcano–ice interactions on Mars: Synthesis of environments and implications for processes and landforms. *Annals of Glaciology*, *45*, 1–13. https://doi.org/10.3189/172756407782282570

Head, J. W., Kreslavsky, M. A., & Pratt, S. (2002). Northern lowlands of Mars: Evidence for widespread volcanic flooding and tectonic deformation in the Hesperian Period. *Journal of Geophysical Research*, *107*(E1), 5003. https://doi.org/10.1029/2000JE001445

Heyer, T., Iqbal, W., Oetting, A., Hiesinger, H., van der Bogert, C. H., & Schmedemann, N. (2023). A comparative analysis of global lunar crater catalogs using OpenCraterTool – An open source tool to determine and compare crater size-frequency measurements [Software]. *Planetary and Space Science*, *231*, 105687. https://doi.org/10.1016/j.pss.2023.105687

Hiesinger, H., & Head, J. W. (2000). Characteristics and origin of polygonal terrain in southern Utopia Planitia, Mars: Results from Mars Orbiter Laser Altimeter and Mars Orbiter Camera data. *Journal of Geophysical Research*, *105*(E5), 11999–12022. https://doi.org/10.1029/1999JE001193

Hiller, K. H. (1979). Geologic map of the Amenthes Quadrangle of Mars: IMAP Report 1110. https://doi.org/10.3133/i1110

Hou, Z., Liu, J., Xu, Y., Pang, F., Wang, Y., Qin, L., et al. (2024). The search for life signatures on Mars by the Tianwen-3 Mars sample return mission. *National Science Review*, *11*, nwae313. https://doi.org/10.1093/nsr/nwae313

Ivanov, B. A. (2001). Mars/Moon cratering rate ratio estimates. *Space Science Reviews*, *96*, 87–104. https://doi.org/10.1007/978-94-017-1035-0_4

Ivanov, M. A., Erkeling, G., Hiesinger, H., Bernhardt, H., & Reiss, D. (2017). Topography of the Deuteronilus contact on Mars: Evidence for an ancient water/mud ocean and long-wavelength topographic readjustments. *Planetary and Space Science*, *144*, 49–70. https://doi.org/10.1016/j.pss.2017.05.012

Ivanov, M. A., Hiesinger, H., Erkeling, G., & Reiss, D. (2014). Mud volcanism and morphology of impact craters in Utopia Planitia on Mars: Evidence for the ancient ocean. *Icarus*, *228*, 121–140. https://doi.org/10.1016/j.icarus.2013.09.018

Jozwiak, L. M., Head, J. W., Zuber, M. T., Smith, D. E., & Neumann, G. A. (2012). Lunar floor-fractured craters: Classification, distribution, origin and implications for magmatism and shallow crustal structure. *Journal of Geophysical Research*, *117*(E11), E11005. https://doi.org/10.1029/2012je004134

Kargel, J. S., Baker, V. R., Begét, J. E., Lockwood, J. F., Péwé, T. L., Shaw, J. S., & Strom, R. G. (1995). Evidence of ancient continental glaciation in the Martian northern plains. *Journal of Geophysical Research*, *100*(E3), 5351–5368. https://doi.org/10.1029/94je02447

Kenkmann, T., Poelchau, M. H., & Wulf, G. (2014). Structural geology of impact craters. *Journal of Structural Geology*, *62*, 156–182. https://doi.org/10.1016/j.jsg.2014.01.015

Komatsu, G., Ori, G. G., Cardinale, M., Dohm, J. M., Baker, V. R., Vaz, D. A., et al. (2011). Roles of methane and carbon dioxide in geological processes on Mars. *Planetary and Space Science*, *59*(2–3), 169–181. https://doi.org/10.1016/j.pss.2010.07.002

Kreslavsky, M. A., & Head, J. W. (2000). Kilometer-scale roughness of Mars: Results from MOLA data analysis. *Journal of Geophysical Research*, *105*(E11), 26695–26711. https://doi.org/10.1029/2000JE001259

Li, C., Zheng, Y., Wang, X., Zhang, J., Wang, Y., Chen, L., et al. (2022). Layered subsurface in Utopia Basin of Mars revealed by Zhurong rover radar. *Nature*, *610*(7931), 308–312. https://doi.org/10.1038/s41586-022-05147-5

Li, J., Liu, H., Meng, X., Duan, D., Lu, H., Zhang, J., et al. (2025). Ancient ocean coastal deposits imaged on Mars. *Proceedings of the National Academy of Sciences*, *122*(9), e2422213122. https://doi.org/10.1073/pnas.2422213122

Liu, J., Ren, X., Yan, W., Chen, W., Zeng, X., Zhang, X., et al. (2024). A 76-m per pixel global color image dataset and map of Mars by Tianwen-1 [Dataset]. *Scientific Bulletin*, *69*(14), 2183–2186. https://doi.org/10.1016/j.scib.2024.04.045

Mangold, N., Adeli, S., Conway, S., Ansan, V., & Langlais, B. (2012). A chronology of early Mars climatic evolution from impact crater degradation. *Journal of Geophysical Research*, *117*(E4), 2011JE004005. https://doi.org/10.1029/2011JE004005

Maxwell, T. A., & McGill, G. E. (1988). Ages of fracturing and resurfacing in the Amenthes region, Mars. In *Lunar and planetary science conference, 18th, Houston, TX, March 16–20, 1987, proceedings (A89-10851 01-91)* (Vol. 18, pp. 701–711). Cambridge University Press/Lunar and Planetary Institute.

McEwen, A. S., Eliason, E. M., Bergstrom, J. W., Bridges, N. T., Hansen, C. J., Delamere, W. A., et al. (2007). Mars reconnaissance Orbiter's high resolution imaging science experiment (HiRISE) [Dataset]. *Journal of Geophysical Research*, *112*(E5), E05S02. https://doi.org/10.1029/2005JE002605

McGill, G. E. (1989). Buried topography of Utopia, Mars: Persistence of a giant impact depression. *Journal of Geophysical Research*, *94*(B3), 2753–2759. https://doi.org/10.1029/JB094iB03p02753

McGill, G. E., & Hills, L. S. (1992). Origin of giant Martian polygons. *Journal of Geophysical Research*, *97*(E2), 2633–2647. https://doi.org/10.1029/91je02863

Melosh, H. J. (1989). *Impact cratering: A geologic process*. Oxford University Press; Clarendon Press. Retrieved from https://ui.adsabs.harvard.edu/abs/1989icgp.book.....M/

Meresse, S., Costard, F., Mangold, N., Masson, P., & Neukum, G. (2008). Formation and evolution of the chaotic terrains by subsidence and magmatism: Hydraotes Chaos, Mars. *Icarus*, *194*(2), 487–500. https://doi.org/10.1016/j.icarus.2007.10.023

Michael, G. (2013). Planetary surface dating from crater size–frequency distribution measurements: Multiple resurfacing episodes and differential isochron fitting [Software]. *Icarus*, *226*(1), 885–890. https://doi.org/10.1016/j.icarus.2013.07.004

Michael, G., Kneissl, T., & Neesemann, A. (2016). Planetary surface dating from crater size-frequency distribution measurements: Poisson timing analysis [Software]. *Icarus*, *277*, 279–285. https://doi.org/10.1016/j.icarus.2016.05.019

Michael, G., & Neukum, G. (2010). Planetary surface dating from crater size–frequency distribution measurements: Partial resurfacing events and statistical age uncertainty [Software]. *Earth and Planetary Science Letters*, *294*(3–4), 223–229. https://doi.org/10.1016/j.epsl.2009.12.041

Michael, G., Platz, T., Kneissl, T., & Schmedemann, N. (2012). Planetary surface dating from crater size–frequency distribution measurements: Spatial randomness and clustering [Software]. *Icarus*, *218*(1), 169–177. https://doi.org/10.1016/j.icarus.2011.11.033

Montmessin, F. (2007). The orbital forcing of climate changes on Mars. *Space Science Reviews*, *125*(1–4), 457–472. https://doi.org/10.1007/s11214-006-9078-x

Nimmo, F., & Tanaka, K. (2005). Early crustal evolution of Mars. *Annual Review of Earth and Planetary Sciences*, *33*(1), 133–161. https://doi.org/10.1146/annurev.earth.33.092203.122637

Osinski, G. R., Lee, P., Parnell, J., Spray, J. G., & Baron, M. (2005). A case study of impact-induced hydrothermal activity: The Haughton impact structure, Devon Island, Canadian High Arctic. *Meteoritics & Planetary Science*, *40*(12), 1859–1877. https://doi.org/10.1111/j.1945-5100.2005.tb00150.x

Osinski, G. R. & Pierazzo, E. (Eds.). (2012). *Impact cratering: Processes and products*. Wiley. https://doi.org/10.1002/9781118447307

Palumbo, A. M., & Head, J. W. (2019). Oceans on Mars: The possibility of a Noachian groundwater-fed ocean in a sub-freezing Martian climate. *Icarus*, *331*, 209–225. https://doi.org/10.1016/j.icarus.2019.04.022

Parker, T. J., Gorsline, D. S., Saunders, R. S., Pieri, D. C., & Schneeberger, D. M. (1993). Coastal geomorphology of the Martian northern plains. *Journal of Geophysical Research*, *98*(E6), 11061–11078. https://doi.org/10.1029/93JE00618

Parker, T. J., Stephen Saunders, R., & Schneeberger, D. M. (1989). Transitional morphology in West Deuteronilus Mensae, Mars: Implications for modification of the lowland/upland boundary. *Icarus*, *82*(1), 111–145. https://doi.org/10.1016/0019-1035(89)90027-4

Ritzer, J. A., & Hauck II, S. A. (2009). Lithospheric structure and tectonics at Isidis Planitia, Mars. *Icarus*, *201*(2), 528–539. https://doi.org/10.1016/j.icarus.2009.01.025

Salvatore, M. R., & Christensen, P. R. (2014). On the origin of the Vastitas Borealis Formation in Chryse and Acidalia Planitiae, Mars: Vastitas Borealis Formation, Mars. *Journal of Geophysical Research: Planets*, *119*(12), 2437–2456. https://doi.org/10.1002/2014JE004682

Schultz, P. H., & Gault, D. E. (1979). Atmospheric effects on Martian Ejecta Emplacement. *Journal of Geophysical Research*, *84*(B13), 7669–7687. https://doi.org/10.1029/JB084iB13p07669

Scott, D. H., & Carr, M. H. (1976). *Geologic map of Mars*. US Geological Survey.

Scott, D. H., & Tanaka, K. L. (1986). Geologic map of the western equatorial region of Mars. *Citeseer*, *1*.

Sharp, R. P. (1973). Mars: Fretted and chaotic terrains. *Journal of Geophysical Research*, *78*(20), 4073–4083. https://doi.org/10.1029/JB078i020p04073

Sholes, S. F., Dickeson, Z. I., Montgomery, D. R., & Catling, D. C. (2021). Where are Mars' hypothesized ocean shorelines? Large lateral and topographic offsets between different versions of paleoshoreline maps. *Journal of Geophysical Research: Planets*, *126*(5), e2020JE006486. https://doi.org/10.1029/2020JE006486

Skinner, J. A., & Tanaka, K. L. (2007). Evidence for and implications of sedimentary diapirism and mud volcanism in the southern Utopia highland–lowland boundary plain, Mars. *Icarus*, *186*(1), 41–59. https://doi.org/10.1016/j.icarus.2006.08.013

Skinner, J. A., & Tanaka, K. L. (2018). *Geologic map of the Nepenthes Planum Region, Mars*. US Geological Survey.

Smith, D. E., Zuber, M. T., Frey, H. V., Garvin, J. B., Head, J. W., Muhleman, D. O., et al. (2001). Mars Orbiter Laser Altimeter: Experiment summary after the first year of global mapping of Mars. *Journal of Geophysical Research*, *106*(E10), 23689–23722. https://doi.org/10.1029/2000JE001364

Solomon, S. C., Aharonson, O., Aurnou, J. M., Banerdt, W. B., Carr, M. H., Dombard, A. J., et al. (2005). New perspectives on ancient Mars. *Science*, *307*(5713), 1214–1220. https://doi.org/10.1126/science.1101812

Squyres, S. W. (1978). Martian fretted terrain: Flow of erosional debris. *Icarus*, *34*(3), 600–613. https://doi.org/10.1016/0019-1035(78)90048-9

Tanaka, K. L. (1997). Sedimentary history and mass flow structures of Chryse and Acidalia Planitiae, Mars. *Journal of Geophysical Research*, *102*(E2), 4131–4149. https://doi.org/10.1029/96je02862

Tanaka, K. L., Carr, M. H., Skinner, J. A., Gilmore, M. S., & Hare, T. M. (2003). Geology of the MER 2003 "Elysium" candidate landing site in southeastern Utopia Planitia, Mars. *Journal of Geophysical Research*, *108*(E12), 2003JE002054. https://doi.org/10.1029/2003JE002054

Tanaka, K. L., Robbins, S. J., Fortezzo, C. M., Skinner, J. A., & Hare, T. M. (2014). The digital global geologic map of Mars: Chronostratigraphic ages, topographic and crater morphologic characteristics, and updated resurfacing history. *Planetary and Space Science*, *95*, 11–24. https://doi.org/10.1016/j.pss.2013.03.006

Tanaka, K. L., Skinner, J. A., & Hare, T. M. (2005). *Geologic map of the northern plains of Mars*. US Geological Survey.

Tanaka, K. L., Skinner, J. A., Hare, T. M., Joyal, T., & Wenker, A. (2003). Resurfacing history of the northern plains of Mars based on geologic mapping of Mars Global Surveyor data. *Journal of Geophysical Research*, *108*(E4), 2002JE001908. https://doi.org/10.1029/2002JE001908

Tanaka, K. L., Skinner Jr., J. A., Dohm, J. M., Irwin III, R. P., Kolb, E. J., Fortezzo, C. M., et al. (2014). *Geologic map of Mars* (p. 43). U.S. Geological Survey Scientific Investigations Map 3292. scale 1:20,000,000, pamphlet. https://doi.org/10.3133/sim3292

Wang, L., & Huang, J. (2024). Hypothesis of an ancient northern ocean on Mars and insights from the Zhurong rover. *Nature Astronomy*, *8*(10), 1220–1229. https://doi.org/10.1038/s41550-024-02343-3

Wang, L., Zhao, J., Huang, J., & Xiao, L. (2023). An explosive mud volcano origin for the pitted cones in southern Utopia Planitia, Mars. *Science China Earth Sciences*, *66*(9), 2045–2056. https://doi.org/10.1007/s11430-022-1119-1

Watters, T. R. (1988). Wrinkle ridge assemblages on the terrestrial planets. *Journal of Geophysical Research*, *93*(B9), 10236–10254. https://doi.org/10.1029/jb093ib09p10236

Watters, T. R., & Robinson, M. S. (1999). Lobate scarps and the Martian crustal dichotomy. *Journal of Geophysical Research*, *104*(E8), 18981–18990. https://doi.org/10.1029/1998je001007

Weiss, D. K., & Head, J. W. (2015). Crater degradation in the Noachian highlands of Mars: Assessing the hypothesis of regional snow and ice deposits on a cold and icy early Mars. *Planetary and Space Science*, *117*, 401–420. https://doi.org/10.1016/j.pss.2015.08.009

Wichman, R., & Schultz, P. (1989). Sequence and mechanisms of deformation around the Hellas and Isidis impact basins on Mars. *Journal of Geophysical Research*, *94*(B12), 17333–17357. https://doi.org/10.1029/jb094ib12p17333

Wilhelms, D. E. (1973). Comparison of Martian and lunar multiringed circular basins. *Journal of Geophysical Research*, *78*(20), 4084–4095. https://doi.org/10.1029/jb078i020p04084

Williams, K. E., Toon, O. B., Heldmann, J. L., & Mellon, M. T. (2009). Ancient melting of mid-latitude snowpacks on Mars as a water source for gullies. *Icarus*, *200*(2), 418–425. https://doi.org/10.1016/j.icarus.2008.12.013

Wilson, L., & Head, J. W. (2004). Evidence for a massive phreatomagmatic eruption in the initial stages of formation of the Mangala Valles outflow channel, Mars. *Geophysical Research Letters*, *31*(15), 2004GL020322. https://doi.org/10.1029/2004GL020322

Wu, B., Dong, J., Wang, Y., Rao, W., Sun, Z., Li, Z., et al. (2022). Landing site selection and characterization of Tianwen-1 (Zhurong rover) on Mars. *Journal of Geophysical Research: Planets*, *127*(4), e2021JE007137. https://doi.org/10.1029/2021JE007137

Xiao, L., Huang, J., Kusky, T., Head, J. W., Zhao, J., Wang, J., et al. (2023). Evidence for marine sedimentary rocks in Utopia Planitia: Zhurong rover observations. *National Science Review*, *10*(9), nwad137. https://doi.org/10.1093/nsr/nwad137

Ye, B., Huang, J., Michalski, J., & Xiao, L. (2019). Geomorphologic characteristics of polygonal features on chloride-bearing deposits on Mars: Implications for Martian hydrology and astrobiology. *Journal of Earth Science*, *30*(5), 1049–1058. https://doi.org/10.1007/s12583-019-1212-2

Yin, A., Wang, Y., & Department of Earth, Planetary, and Space Sciences, University of California, Los Angeles, CA 90095-1567, USA. (2023). Formation and modification of wrinkle ridges in the central Tharsis region of Mars as constrained by detailed geomorphological mapping and landsystem analysis. *Earth and Planetary Physics*, *7*(2), 161–192. https://doi.org/10.26464/epp2023031

Zhang, T., Huang, J., Wang, L., Wueller, L., Iqbal, W., Liu, J., et al. (2025). Geological history of the dichotomy in the southern Utopia Planitia of Mars [Dataset]. *Zenodo*. https://doi.org/10.5281/zenodo.16517287

Zhang, T., Wang, L., Saidamat, A., Xiao, L., & Huang, J. (2023). Evolution history of Mesas in the southern Utopia Planitia and implications for the ancient oceans on Mars. *Journal of Earth Science*, *34*(3), 940–950. https://doi.org/10.1007/s12583-022-1776-0

Zhao, J., Xiao, Z., Huang, J., Head, J. W., Wang, J., Shi, Y., et al. (2021). Geological characteristics and targets of high scientific interest in the Zhurong landing region on Mars. *Geophysical Research Letters*, *48*(20), e2021GL094903. https://doi.org/10.1029/2021GL094903